Under-ice phytoplankton bloom dynamics controlled by spring convective mixing in refreezing leads of open water

K. E. Lowry[1,2]†, R. S. Pickart[2], V. Selz[1], M. M. Mills[1], A. Pacini[2], K. M. Lewis[1], H. Joy-Warren[1], C. Nobre[2], G. L. van Dijken[1], P.-L. Grondin[3], J. Ferland[3], and K. R. Arrigo[1]

[1]Earth System Science Department, Stanford University, 473 Via Ortega, Stanford, CA, 94035.
[2]Woods Hole Oceanographic Institution, Woods Hole, MA, 02543.
[3]Université Laval, Québec, QC, G1V 0A6, Canada.

Corresponding author: Kate E. Lowry (lowryk@alumni.stanford.edu)
†Present address: Woods Hole Oceanographic Institution, MS #29, Woods Hole, MA, 02543

Key Points:

- Spring phytoplankton blooms were present beneath fully consolidated sea ice with snow
- Under-ice phytoplankton biomass was inversely correlated with lead fraction
- Convection in refreezing leads enhances mixing and controls under-ice bloom dynamics

Abstract

Spring phytoplankton growth in polar marine ecosystems is limited by light availability beneath ice-covered waters, particularly early in the season prior to snowmelt and melt pond formation. Leads of open water increase light transmission to the ice-covered ocean and are sites of air-sea exchange. We explore the role of leads in controlling phytoplankton bloom dynamics within the sea ice zone of the Arctic Ocean. Data are presented from spring measurements in the Chukchi Sea during the Study of Under-ice Blooms In the Chukchi Ecosystem (SUBICE) program in May-June 2014. We observed that fully consolidated sea ice supported modest under-ice blooms, while waters beneath sea ice with leads had significantly lower phytoplankton biomass, despite high nutrient availability. Through an analysis of hydrographic and biological properties, we attribute this counterintuitive finding to springtime convective mixing in refreezing leads of open water. Our results demonstrate that waters beneath loosely consolidated sea ice (e.g. 85-95% ice concentration) had weak stratification and were frequently mixed below the critical depth (the depth at which depth-integrated production balances depth-integrated respiration). These findings are supported by theoretical model calculations of under-ice light, primary production, and critical depth at varied lead fractions. The model demonstrates that under-ice blooms can form even beneath snow-covered sea ice in the absence of mixing but not in more deeply mixed waters beneath sea ice with refreezing leads. Future estimates of primary production should account for these phytoplankton dynamics in ice-covered waters.

1 Introduction

Each year, the physical environment of the Arctic Ocean undergoes seasonal changes in solar irradiance and sea ice cover that drive the productivity of the marine ecosystem *[Loeng et al.*, 2005]. While winter is characterized by darkness and expansive sea ice, in summer the region receives up to 24 hours of sunlight per day and contains large stretches of open water [*Parkinson and Cavalieri*, 2008], particularly in Arctic continental shelf seas [*Arrigo et al.*, 2008]. Sunlight and sea ice extent wax and wane during transition periods; as the intensity of solar radiation decreases in fall, sea ice cover advances, while an increase in solar radiation in spring is accompanied by sea ice melt. Physical and biogeochemical properties of seawater are highly dynamic over the annual cycle, yet relatively understudied in non-summer months due to the difficulty of sampling ice-covered waters via ship or satellite.

During the advance of sea ice cover in the fall, salt is excluded from freezing seawater through brine rejection, producing a layer of relatively fresh sea ice. The excluded cold, saline, and dense brine sinks in the ocean to its density equilibrium and is replaced by more buoyant seawater through convection, thereby mixing the water column. Brine rejection and subsequent convective mixing continues through the winter as more sea ice is produced in areas of open water such as sea ice leads and polynyas [*Smith and Morison*, 1993; *Weingartner et al.*, 1998; *Pickart et al.*, 2016]. These physical winter processes form the dense near-freezing (potential temperature ≤ -1.6°C) water mass referred to as winter water (WW).

On shallow shelves such as the Chukchi Sea and the Bering shelf, convective mixing can completely overturn the water column and lead to exchange with remineralized benthic nutrients, resulting in a relatively uniform and extremely nutrient-rich water mass [*Lowry et al.*, 2015; *Pacini et al.*, submitted; *Pickart et al.*, 2016]. In the summer, the WW is increasingly modified through solar heating and/or lateral mixing [e.g. *Gong and Pickart*, 2016] and biological activity [*Lowry et al.*, 2015], and is eventually transported northward to the deep Arctic basin. This occurs via advection through Barrow Canyon [*Woodgate et al.*, 2005b; *Itoh et al.*, 2012; *Gong and Pickart*, 2015; *Itoh et al.*, 2015] and Herald Canyon [*Pickart et al.*, 2010]. The WW is also fluxed offshore via turbulent processes such as eddy formation in the two canyons [*Pickart et al.*, 2005; *Pisareva et al.*, 2015] and eddy generation from the shelfbreak jet along the Chukchi and Beaufort Seas [*Spall et al.*, 2008; *Mathis et al.*, 2007]. As the season progresses, WW on the

Chukchi shelf is replaced by warmer, fresher, nutrient-poor Pacific summer water [e.g. *Woodgate et al.*, 2005a; *Cooper et al.*, 1997].

Field work as part of the NASA-funded Impacts of Climate on EcoSystems and Chemistry of the Arctic Pacific Environment **(**ICESCAPE) program in the Chukchi Sea in June-July 2010 and 2011 [*Arrigo*, 2015; 2016] confirmed that WW is a significant nutrient source for phytoplankton at the base of the marine food web. An analysis of hydrographic sections and biogeochemical properties in the Chukchi Sea revealed that WW was consistently associated with summer phytoplankton blooms of great magnitude and duration [*Lowry et al.*, 2015]. Concentrations of nitrate, the primary limiting nutrient for phytoplankton growth in the Arctic [*Cota et al.*, 1996; *Codispoti et al.*, 2005; *Tremblay and Gagnon*, 2009], were 10-fold higher in WW (e.g. >10 µmol L^{-1}) than in adjacent water masses [*Lowry et al.*, 2015], demonstrating the importance of WW as the primary source of nutrients for growth by phytoplankton. Further, the complex flow paths of the Chukchi Sea extend the residence time of nutrient-rich WW on the shelf [*Pickart et al.*, 2016], which likely plays a critical role in sustaining the region's immense phytoplankton blooms [*Lowry et al.*, 2015] and biological hotspots [*Grebmeier et al.*, 2015].

Climate change has dramatically transformed the Arctic Ocean in recent decades, with important implications for the marine ecosystem. In particular, the seasonal cycle of sea ice retreat and advance has intensified, with more ice melting each year and returning as thin first-year sea ice rather than the once-prevalent thick multi-year ice [*Maslanik et al.*, 2011]. Sea ice in this region retreated up to two months earlier and advanced more than a month later in 2010-11 as compared to 1979-80 [*Stammerjohn et al.*, 2012], corresponding to up to a three month increase in the open water growing season. Open water phytoplankton primary production increased by 42% in the Chukchi Sea from 1998 to 2012, according to satellite estimates [*Arrigo and van Dijken*, 2015]. An unprecedented and massive under-ice bloom was observed during ICESCAPE in the Chukchi Sea [*Arrigo et al.*, 2012], indicating the suitability of the under-ice environment for phytoplankton growth. The presence of melt ponds on the fully consolidated sea ice (Fig. 1a), which transmit up to 55% of the incident irradiance to the underlying water column [*Frey et al.*, 2011], supported extremely high growth rates and phytoplankton biomass within the bloom [*Arrigo et al.*, 2014; Fig. 1b]. Enhanced under-ice phytoplankton biomass has been observed elsewhere as well [*Legendre et al.*, 1981; *Yager et al.*, 2001; *Fukuchi et al.*, 1989; *Strass and Nöthig*, 1996; *Fortier et al.*, 2002; *Mundy et al.*, 2009; *Assmy et al.*, 2017].

Descriptions of phytoplankton bloom dynamics in the Arctic Ocean typically attribute the onset of the spring phytoplankton bloom to increased light availability and water column stratification following sea ice melt. ‘Marginal ice zone’ or ‘ice-edge’ blooms forming in this way are described as ubiquitous in the Arctic Ocean and considered to be substantial contributors to total primary production in this region [*Hameedi*, 1978; *Perrette et al.*, 2011]. Previous field observations in the Chukchi Sea in May-June (spring) and July-August (summer) of 2002 and 2004 as part of the Shelf-Basin Interactions (SBI) project support this concept. For example, hydrographic measurements indicated that waters were relatively well-mixed with high pre-bloom nutrient concentrations beneath sea ice in spring and more stratified with lower nutrient concentrations in summer [*Codispoti et al.*, 2005, 2009], with nutrient depletion attributed to a spring phytoplankton bloom [*Hill et al.*, 2005]. *Sukhanova et al.* [2009] found phytoplankton biomass across the shelf in 2002 to be an order of magnitude higher in waters with reduced sea ice cover (<50%) in summer than in waters with greater ice cover (>80%) in spring. These and other SBI measurements have been critically important for understanding spring and summer physical and biological processes in the Chukchi Sea. However, fully characterizing under-ice hydrography and nutrients and phytoplankton dynamics requires additional early season observations.

Motivated by the need to better understand phytoplankton blooms in the sea ice zone, the NSF-funded Study of Under-ice Blooms In the Chukchi Ecosystem (SUBICE) program took place in May-June 2014, resulting in an extensive late-spring study of hydrography, nutrients, and phytoplankton beneath the ice in the Chukchi Sea. The field sampling was primarily during pre-bloom conditions prior to melt pond formation. Leads of open water were prevalent throughout the study area. Ranging by definition in size from 50 m up to several kilometers or even hundreds of kilometers (World Meteorological Association), leads are elongated and recurring areas of open water and thin sea ice (illustrated in Fig. 1c) and are important sites for air-sea-ice-ocean interactions [*Willmes and Heinemann*, 2016]. Leads act as windows [*Pegau and Paulson*, 2001] for solar radiation to penetrate the otherwise dark water column (Fig. 1d) beneath snow-covered ice, which strongly attenuates sunlight [*Perovich*, 2002].

In this study, we investigate the mechanisms controlling phytoplankton bloom development in ice-covered waters in late-spring, with particular emphasis on the role of leads in the sea ice. By combining an analysis of SUBICE field observations with satellite sea ice imagery and a theoretical model of irradiance and primary production at varied ice concentrations, we explore the influence of open water leads on phytoplankton growth in the sea ice zone. In particular, we test the hypothesis that blooms can form in the snow-covered sea ice zone when leads are present. This work is critical for improving our knowledge of under-ice phytoplankton dynamics.

2 Materials and Methods

2.1 Data collection

2.1.1 Field sampling and laboratory analysis

Aboard USCGC *Healy*, the SUBICE field campaign (13 May – 23 June 2014) sampled 230 hydrographic stations primarily on the continental shelf of the northeastern Chukchi Sea (Fig. 2). Conductivity-temperature-depth (CTD) casts were made using dual temperature (SBE3), conductivity (SBE4c), and pressure (Digiquartz 0-10,000 psi) sensors attached to the ship's rosette system, with uncertainty estimates of 0.001°C for temperature and 0.008 for salinity. Additional sensors included dissolved oxygen (SBE43), photosynthetically active radiation (PAR) (Biospherical QSP-2300), fluorescence (WET Labs ECO-AFL/FL), and beam transmission (WET Labs C-Star). Currents were measured using the ship's hull-mounted Acoustic Doppler Current Profiler (ADCP) system. We also measured sea ice thickness, snow depth, and ice algal properties at select locations. Field methods are described in more detail in *Arrigo et al.* [2017] for water column sampling and *Selz et al.* [2017] for sea ice sampling.

Discrete seawater samples were collected at standard depths (2, 5, 10, 25, 50, 75, and 100 m) in addition to the depth of the subsurface fluorescence maximum (if present) and 2-3 m from the seafloor bottom. Seawater samples were analyzed for a suite of biogeochemical and biological parameters. Nutrient analysis was performed onboard using a Seal Analytical continuous flow Auto-Analyzer 3 and a modification of the method of *Armstrong et al.* [1967]. Seawater samples for dissolved oxygen (O_2) and salinity were analyzed for sensor calibration.

For analysis of chlorophyll *a* (Chl *a*) concentration, seawater was filtered onto 25 mm Whatman GF/F filters of 0.7 µm nominal pore size. The filters were extracted in the dark in 5 mL of 90% acetone for 24 hrs at +3°C prior to measurement [*Holm-Hansen et al.*, 1965] on a Turner Designs 10-AU fluorometer calibrated with pure Chl *a* (Sigma). While we also measured particulate organic carbon and nitrogen (POC and PON), we relied exclusively on Chl *a* because it is a less ambiguous indicator of phytoplankton biomass than POC at low concentrations.

Phytoplankton physiology was assessed using a fast repetition rate fluorometer (FRRf) with excitation at 470 nm to measure the maximum efficiency of photosystem II (Fv:Fm) of seawater samples [*Kolber et al.*, 1998], which provides an indication of phytoplankton 'health'. Samples were dark-acclimated for ~30 minutes at *in situ* temperature and measured in triplicate within one hour of collection. Fv:Fm blanks for each sample were measured after gentle filtration via 0.2 µm polycarbonate syringe filter [*Cullen and Davis*, 2003].

Phytoplankton photosynthetic parameters were determined at the surface and subsurface (typically 10 or 25 m depth) from photosynthesis (P) versus irradiance (E) curves following the P-E method of *Lewis and Smith*, [1983], modified and detailed by *Arrigo et al.* [2010]. Seawater samples labeled with ^{14}C-bicarbonate were incubated under a range of light levels (0 to 522 µEin m^{-2} s^{-1}) and later assayed for ^{14}C incorporation using a Perkin Elmer WinSpectral 1414 liquid scintillation counter. The resultant P-E curves provide estimates of maximum Chl *a*-normalized (*) photosynthetic rates (P^*_{max}) (mg C mg^{-1} Chl *a* h^{-1}), light limited efficiency of photosynthesis (α^*) (mg C mg^{-1} Chl *a* h^{-1} (µEin m^{-2} s^{-1})$^{-1}$), and the light-saturation intensity parameter (E_K) (µEin m^{-2} s^{-1}), after correcting for the amount of carbon uptake/release at 0 µEin m^{-2} s^{-1}. P-E curves were fit to the model of *Webb et al.* [1974]. The model of *Platt et al.* [1981] that includes photoinhibition (β) was considered but disregarded due to insignificant β values for this study.

Community composition was assessed via Imaging FlowCytobot analysis to determine the relative contributions (mean ± SD) of water column phytoplankton versus ice-derived algal diatoms to the biomass observed at two bloom locations. We followed the method of *Selz et al*. [2017], although in our case water samples were pre-filtered using 150 µm Nitex mesh. Small unidentified cells, flagellates, and dinoflagellates were excluded from classification. A total of 476 images from four stations were classified. As in *Laney and Sosik* [2014], colonies and chains of diatoms were each counted as one image rather than multiple individual cells.

2.1.2 Sea ice concentration and lead fraction

Daily satellite images from the Special Sensor Microwave Imager (SSM/I) at 25 km resolution were obtained from the National Snow and Ice Data Center [*Cavalieri et al.*, 1996] and used to characterize the sea ice concentration at each hydrographic station for the date it was sampled. The uncertainty for highly concentrated non-ponded sea ice is <5% [*Cavalieri et al.*, 1996] (http://nsidc.org/data/docs/daac/nsidc0051_gsfc_seaice.gd.html). During the cruise, sea ice concentration was also estimated visually through 'ice watch' observations every two hours made from *Healy's* bridge. Because satellite ice concentrations correlated well with *in situ* observations (R=0.83; slope=0.67; p<0.01), we used only satellite-derived sea ice concentrations in this study to represent a large spatial area surrounding each hydrographic station. The presence of leads at each station was determined via satellite from the amount of open water and is referred to as the lead fraction (i.e. the inverse of sea ice fraction). We note that lead fraction, rather than lead size, is a relevant indicator of light transmission to ice-covered waters.

2.2 Data analysis

2.2.1 Station selection

This study focuses solely on phytoplankton bloom development originating in ice-covered waters. Satellite ocean color imagery from MODIS Aqua revealed the presence of an open water phytoplankton bloom located northwest of Bering Strait and roughly centered at 67.5°N, 170°W, south and upstream of our study region. To eliminate the potential influence of the advection of this open water phytoplankton bloom from our study, we estimated the date a parcel of northward flowing water from the bloom would reach the latitude of each station. To be conservative we chose a current speed of 17.5 cm s^{-1}, a rate equivalent to the fastest northward flowing current observed during SUBICE, and assumed a straight-line distance, resulting in the shortest possible travel time to each station. Stations sampled after the respective dates were flagged as potentially influenced by advection of open water phytoplankton and removed from the analysis. We also flagged 10 stations near the coast as potentially influenced by advection of open water phytoplankton along the northeastward flowing Alaska Coastal Current or by nearshore processes such as upwelling. The remaining 72 stations are the focus of this study (Fig. 2), comprising seven transects across a latitudinal range of ~70.7 – 73.3°N and a date range of 18 May – 2 June 2014. The bottom depth of the stations ranged from 36 to 195 m. We note that the southernmost section was sampled early in the cruise, after which the ship headed northeast. The additional removed stations were generally sampled later in the cruise.

2.2.2 Water column structure

Using CTD density profiles, we calculated the surface mixed layer depth (MLD) and the bottom mixed layer depth at each station following the procedure described in *Pickart et al.* [2002] and *Våge et al.* [2015]. During SUBICE, most of the northeast Chukchi shelf was characterized as a two-layer system with a surface mixed layer atop a bottom mixed layer, separated by a thin density interface. We refer to the magnitude of density jump between the top and bottom mixed layers as the stratification index. At stratification index < 0.01 kg m^{-3}, the water column was considered well mixed from top to bottom (i.e. recently overturned; *Pacini et al.* [submitted]).

2.2.3. Primary production, community respiration, and critical depth

Rates of daily gross primary production (GPP) were estimated for under-ice phytoplankton using measured P-E parameters and irradiance at 1 m depth intervals. Daily cycles of irradiance were based on the hourly mean incident surface PAR from the ship's mast. Light transmission to the ocean was calculated based on the satellite-derived ice concentration at each station and modeled light attenuation through ice and leads (Section 2.3). CTD profiles of corrected PAR (%) were used to compute water column light transmission. Normalized photosynthetic rates (P*) at varying irradiance (E) were calculated from mean P-E parameters. P* (mg C mg^{-1} Chl *a* m^{-3} h^{-1}) and depth profiles of Chl *a* were used to estimate GPP (mg C m^{-3} d^{-1}). Total depth-integrated GPP (mg C m^{-2} d^{-1}) was calculated over a daily cycle for each station.

Community respiration was estimated based on the difference in apparent oxygen utilization (AOU), or the deficit in dissolved O_2 relative to saturation, between two sets of stations along the northward-flowing branch of Pacific-origin water called the Central Channel pathway (Fig. 2; e.g. *Weingartner et al*. [2005]; *Gong and Pickart* [2015]). As detailed in *Lowry* (2016), we estimate a range of respiration rates of 4.4 - 6.6 mg C m^{-3} d^{-1}, which compares well with observed rates [e.g. *Cottrell et al.*, 2006] and approximates seasonal variation as primary production increases. Thus, we use our lower estimate of community respiration to simulate pre-bloom conditions before the cruise and the upper estimate for calculating critical depth during the cruise. We estimate net community production (NCP) as community respiration minus GPP.

The critical depth (Z_{cr}) at each station was defined as the depth where depth-integrated primary production balanced depth-integrated community respiration [*Sverdrup*, 1953]. Our depth-integrated GPP and community respiration estimates were used to calculate Z_{cr} as the depth above which net growth processes of phytoplankton balance net loss processes via grazing, bacterial remineralization, and mortality. When theoretical Z_{cr} exceeded the bottom depth, Z_{cr} was set to the bottom depth to calculate a mean. We also computed euphotic depth (1% light level) but present only Z_{cr} because it is more relevant for ice-covered waters.

2.2.4 Hydrographic sections

For the seven SUBICE transects considered in this study (Fig. 2), vertical sections of hydrographic properties were constructed using a Laplacian-spline interpolator, as in *Pickart et al.* [2016]. We present potential temperature (θ) and potential density referenced to the sea surface, salinity, nitrate (NO_3^-), Chl *a*, O_2 saturation, and Fv:Fm. To visualize the vertical extent of mixing and light availability relative to phytoplankton biomass, sections of Chl *a* are overlain with lines indicating the MLD and Z_{cr}. Hydrographic sections are displayed with geographical context maps and plots of sea ice concentration and the stratification index along each section.

2.2.5 Statistical analyses

To assess how sea ice concentration, water column structure, and environmental conditions control biological and biogeochemical properties, we performed single and multiple linear regression analyses. Depth-integrated means of biological variables were calculated for the mixed layer (ML) and the full water column for statistical analysis. Correlations between variables were determined through Pearson's correlations using Student's t distributions for transformation of the correlations. We also performed t-tests to compare means of water column structure properties at extremely high ice concentration (≥98%) versus sea ice with leads.

A multiple linear regression model was developed to understand the relative importance of physical and environmental variables in predicting ML phytoplankton biomass. The relative importance of each variable was quantified as the percent of R^2 explained using the relaimpo R package [*Grömping*, 2006]. Chl *a* was log-transformed and we assessed the potential for multicollinearity of predictor variables by the condition number [*Belsley et al.*, 1980] less than 3.

2.3 Model of irradiance, production, and critical depth beneath sea ice with leads

To investigate how leads of open water might influence phytoplankton growth beneath snow-covered sea ice, we constructed a theoretical model of water column PAR, GPP, and Z_{cr}. The model simulates incident PAR transmission through sea ice and leads, the daily solar cycle for waters advecting beneath ice with leads, and under-ice GPP and Z_{cr} at varied lead fractions. The model description is presented in more detail in *Lowry* (2016).

2.3.1. Transmission of incident PAR through sea ice and the water column

We use mean hourly surface PAR measurements from 18 May – 2 June 2014 to simulate the daily light cycle. To calculate light transmission to ice and open water, specular reflection was set at 5% for the atmosphere-snow interface and calculated as a function of solar zenith angle for open water [*Kirk*, 2010], assuming a flat ocean surface (there are few waves in leads).

Light transmission was calculated through snow/sea ice assuming attenuation through a layer of snow on the ice and a layer of algae in the bottom 0.02 m of the ice. The following attenuation coefficients for PAR were used for dry snow, interior white ice, and sea ice algae: $K_{d\ snow} = 21.4$ m^{-1}, $K_{d\ ice} = 1.59\ m^{-1}$, and $K_{d\ algae} = 10.0\ m^{-1}$ [*Perovich,* 1990; *Perovich et al.,* 2007]. Irradiance (E_0) (µEin $m^{-2}\ s^{-1}$) was transmitted through the snow, ice, and algal layers using Beer's Law:

$$E_z = E_0 * exp^{-K_d * z} \tag{1}$$

where z is the layer thickness and K_d is the attenuation coefficient for that layer. A snow depth of 0.07 m was used to represent early season pre-bloom conditions, prior to the additional spring snow accumulation we observed during SUBICE (e.g. 0.09 m snow depth). Thicknesses of sea ice (1.12 m) and the ice algal layer (0.02 m) represent mean observed conditions. Light transmission in the water column was calculated as a function of Chl *a* [*Morel*, 1988]:

$$K_{d\ water} = 0.04 + 0.05 * Chl\ \mathrm{a}^{0.681}. \tag{2}$$

2.3.2. Simulating advection of waters beneath sea ice and open water leads

Because highly concentrated pack-ice can become fast or quasi-stationary, the model accounts for the advection of water beneath sea ice cover of a given lead fraction by assuming a 24-hour daily cycle at a fixed location with alternating periods of ice and open water. Leads were simulated as hourly increments of open water within the sea ice. For example, 100% ice concentration was simulated as a daily cycle with 24 hrs of sea ice and zero hrs of open water, while ~92% ice concentration was simulated as a daily cycle with 22 hrs of sea ice and two hrs of open water. Variation in total light transmitted based on the time of day of the leads and the lead interval size was controlled by randomly distributing the time when leads were present and running 50,000 simulations for each lead fraction. This design approximates realistic conditions in which phytoplankton are advected beneath leads of varying size and at varying times of day relative to solar noon. For each simulated daily cycle, PAR was transmitted through snow, ice, and algae during sea ice intervals and through open water during lead intervals.

2.3.3 GPP and Z_{cr} simulations at varied lead fractions

For each daily cycle of sea ice and leads, GPP was estimated at each depth based on simulated PAR and mean P-E parameters for under-ice phytoplankton. Daily GPP (mg C $m^{-3}\ d^{-1}$) was calculated assuming a uniformly low phytoplankton abundance (0.1 mg Chl *a* m^{-3}) for pre-bloom conditions. This value was the minimum concentration in the upper 20 m measured during SUBICE. Daily GPP profiles were computed from model means and standard deviations for each lead fraction and used to simulate Z_{cr} based on pre-bloom respiration and an unconstrained bottom.

3 Results

3.1 Physical environment

3.1.1 Sea ice cover

The Chukchi Sea was characterized by extensive sea ice cover with numerous leads of open water during our early season sampling period in May-June 2014. Visual ice watch observations revealed that the vast majority of openings in the sea ice were narrow breaks ranging in size from <50 m to 200 m. While sea ice concentrations were high at all 72 stations, with a satellite-derived mean of 95.5 ± 3.6%, there was regional variation (Fig. 3a). The eastern stations had the highest sea ice concentrations (95-100%) and therefore the fewest leads, while the central and southern stations had relatively lower sea ice concentrations (84-95%) with more open water leads. Observations from the ship's bridge and field measurements during the ice stations indicated that the dominant type of ice was first-year sea ice that had formed during the previous winter. Based on the seven ice stations that were conducted over the time period of this analysis, first-year sea ice thickness ranged from 0.43 to 1.50 m, with an average thickness of 1.12 ± 0.37 m. Snow depth on first-year sea ice ranged from 0.05 to 0.15 m, with an average depth of 0.09 ± 0.04 m. The bottom 0.02 m of the sea ice frequently harbored a layer of sea ice algae (*Selz et al.* [2017]). There were no melt ponds on the sea ice. Frequent refreezing of open water leads was observed during the cruise, consistent with the cold air temperatures (as cold as -5 to -7°C).

3.1.2 Hydrography and water column structure

The shallow water column of the Chukchi Sea consisted almost exclusively of near-freezing WW. The mean θ across all 72 stations and over all depths was -1.71 ± 0.05°C, and the mean salinity was 32.1 ± 0.54. During the spring sampling period, the Chukchi Sea was generally characterized as a weakly stratified two-layer system, with an upper mixed layer and a bottom boundary layer separated by an interface between the two layers. The stratification index was very low for waters on the shelf (Fig. 3b), revealing that much of the Chukchi Sea was weakly stratified. By contrast, the stations occupied in the vicinity of the shelfbreak in the northern part of our sampling domain had a higher stratification index. Here the presence of slightly warmer and fresher basin water resulted in stronger vertical density gradients.

Notably, the water column was deemed fully mixed at seven stations on the shelf where the stratification index was <0.01 kg m^{-3} (marked by asterisks in Fig. 3b; note that two fully mixed stations were excluded in the advection flagging process). This, together with the consistently low stratification index on the shelf, suggests that the water column was actively overturning during our shipboard survey. This hypothesis was addressed by *Pacini et al.* [submitted] who used a polynya model with a 1-D mixing model to investigate the likelihood for convection to reach the bottom. The idea is that brine rejection within the many refreezing leads would lead to convective overturning that could erode the interface and cause the surface and bottom mixed layers to merge. The polynya model was forced by realistic surface heat loss for the time of the cruise, and the resulting negative freshwater flux (i.e. brine rejection) was applied to all of the CTD profiles occupied on the northeast shelf using the mixing model. *Pacini et al.* [submitted] found that, on average, the water column would be completely mixed in less than 9 hours (in some cases the overturn time was less than an hour), offering strong support for the convective hypothesis. Other factors could also contribute, such as wind-induced mixing. Using a numerical model, *Martin et al*. [2014] found that the ice-ocean stress is enhanced for partial ice concentration (versus a full ice cover or near-open water). This would favor mixing of the upper water column in regions of numerous leads. However, winds were generally light during SUBICE, and the optimal ice concentration for such mixing is 80-90%, on the low end of concentrations observed during SUBICE. MLD ranged from 8 to 60 m across the domain, with a mean of 30 ± 9.1 m (Fig. 3c); however, there were no obvious spatial patterns, consistent with the notion of stochastically forced convection.

3.2 Nutrients, phytoplankton, and critical depth

Nutrient concentrations during SUBICE were very high throughout the Chukchi Sea, consistent with the widespread presence of near-freezing WW, which is generally rich in nutrients. Across all 72 stations (n=387), the mean NO_3^- concentration was 11.2 ± 3.58 µmol L^{-1}, ranging from 0.42 to 17.0 µmol L^{-1}. Within the upper mixed layer, the mean NO_3^- concentration was 10.9 ± 3.70 µmol L^{-1}. Concentrations of PO_4^{3-} and $Si(OH)_4$ were also very high, with means of 1.77 ± 0.32 µmol L^{-1} and 44.2 ± 12.7 µmol L^{-1}, respectively. These extremely high nutrient concentrations suggest that phytoplankton growth was not limited by macronutrients.

Despite high nutrient availability, phytoplankton biomass was relatively low at most stations. The mean water column Chl *a* concentration across all samples was 0.40 ± 0.38 µg L^{-1}. Overall mean ML Chl *a* concentration was 0.46 ± 0.36 µg L^{-1}, with station ML means ranging from 0.13 to 1.88 µg Chl *a* L^{-1}. Consistent with low phytoplankton biomass, O_2 was generally undersaturated, with a mean O_2 of 87.2 ± 5.66% (ranging from 76.1 to 104%).

The photosynthetic parameters for under-ice phytoplankton were P^*_m = 4.41 ± 2.19 mg C mg^{-1} Chl *a* hr^{-1} and α^* = 0.106 ± 0.068 mg C mg^{-1} Chl *a* hr^{-1} (µEin m^{-2} $s^{-1})^{-1}$ (N=7), which were used to calculate GPP. The corresponding E_K was 59.4 ± 52.9 µEin m^{-2} s^{-1}. On average, the mean Fv:Fm was 0.31 ± 0.12 (N=99), with a range of 0.02-0.54.

Estimates of depth-integrated GPP at each station ranged from 0.03 to 0.86 g C m^{-2} d^{-1}, with a mean of 0.20 ± 0.14 g C m^{-2} d^{-1}. After subtracting community respiration at each depth, the resulting estimated depth-integrated NCP ranged from -1.14 to 0.65 g C m^{-2} d^{-1}, with a mean of -0.15 ± 0.21 g C m^{-2} d^{-1}. These under-ice production estimates illustrate that community respiration largely exceeded gross primary production during our early season sampling period.

Z_{cr} ranged from 3 to 64 m (Fig. 3d) and was deepest on the southern and outer shelf and shallowest on the central shelf of the Chukchi Sea. There were eight stations where theoretical Z_{cr} exceeded the bottom depth. The mean Z_{cr} (26 ± 14 m) was ~4 m shallower than the mean MLD.

3.3 Hydrographic sections

To illustrate controls on under-ice phytoplankton blooms in the spring, we present hydrographic sections of physical and biological properties for three of the seven transects in chronological order. These sections were chosen because they represent the range of conditions encountered during the survey. The remaining four transects are presented in *Lowry* (2016) (available at https://purl.stanford.edu/vz619fm8134; pp. 98-109).

Hanna Ridge Section

Of the seven transects sampled, three contained under-ice phytoplankton blooms. The most intense bloom was located on the Hanna Ridge transect, sampled 22-23 May 2014 (Fig.

4a). Fully consolidated sea ice with few to no leads (98-100%) covered all stations except the northernmost and southernmost endpoints (St. 41 and 34), which had 96-97% ice concentration (Fig. 4b). The stratification index (Fig. 4b) was very low (0.10-0.12 kg m^{-3}) at the endpoints and higher (0.25-0.57 kg m^{-3}) at the interior stations with 100% ice cover. ML slope followed the same pattern, indicating a greater degree of stability within the upper mixed layer beneath the fully consolidated ice. Like most of the region, the water column was composed entirely of near-freezing WW ($\theta \leq -1.6°C$) (Fig. 4c). At these cold temperatures the stratification is dominated by salinity; accordingly, salinity was more vertically uniform at the endpoints, with a stronger vertical gradient at the interior stations (Fig. 4d).

Nutrient concentrations were extremely high throughout the water column, with a range of ~13-17 µmol NO_3^- L^{-1} (Fig. 4e). A ~60 km wide under-ice phytoplankton bloom was present in the more stable waters beneath the fully consolidated sea ice (Fig. 4f), with the highest concentrations of Chl a within the upper 10 m of the interior stations (particularly St. 40-38), with values of ~1-3 µg L-1. The diatom community within the bloom (St. 37 and 38) was composed primarily of water column phytoplankton (*Chaetoceros*, *Thalassiosira*, *Cylindrotheca, Navicula pelagica,* and unidentified centrics) with a relative abundance of 62 ± 14%, as compared to 38 ± 14% for ice algal diatoms (large unidentified pennates and *Nitzschia* spp.). The bloom extended to the MLD (~25 m; purple dotted line), while Z_{cr} (grey dotted line) extended beyond the seafloor (>45 m; Fig. 4f). Oxygen was undersaturated throughout the water column but highest (~90%) within the bloom (Fig. 4g). Fv:Fm, which indicates photosynthetic efficiency or phytoplankton ‘health’, was also highest (>0.45) within bloom (Fig. 4h). Biomass was lowest at the weakly stratified endpoint stations with relatively more open water leads.

Chukchi Northwest Section

In contrast to the above scenario, phytoplankton biomass was consistently low (e.g. 0.2-0.4 µg Chl a L^{-1}) along multiple transects. This is nicely illustrated by the Chukchi Northwest transect (Fig. 5a), which was sampled 24-25 May 2014 after the Hanna Ridge transect. Leads of open water were present at all stations (92-94% ice concentration) and the stratification index was relatively low (<0.4 kg m^{-3}) across the transect, especially at the southernmost stations (0.05-0.1 kg m^{-3}) (Fig. 5b). Vertically homogeneous hydrographic properties (Figs. 5c-d) in the loosely consolidated ice pack are consistent with the occurrence of recent convective mixing.

Nutrient concentrations were high (9-14 µmol NO_3^- L^{-1}) in the near-freezing WW, particularly in the near-bottom salty water on the outer part of the transect corresponding to the seaward edge of a flow pathway (Fig. 2). Despite these high nutrient values, phytoplankton biomass was low (<0.4 µg Chl *a* L^{-1}) and MLD exceeded Z_{cr} at all stations except St. 51, where MLD and Z_{cr} were nearly equal (Fig. 5e-f). Oxygen was undersaturated (76-92%) and Fv:Fm was relatively low (<0.4) at most stations (Figs. 5g-h).

Central Shelf Section

A third scenario, corresponding to a pronounced cross-shelf gradient of physical and biological properties, was observed along the Central Shelf transect. This section was sampled 31 May – 2 June 2014, several days after the Chukchi Northwest transect, and extended southwest from the continental slope to the central Chukchi shelf (Fig. 6a). The northern half of the transect contained fully consolidated sea ice with very few leads (98-100% ice concentration) and was highly stratified (index: ~1-3 kg m^{-3}) due to the shelfbreak front separating WW on the shelf from the warmer, fresher water over the slope. Sections of θ and salinity (and hence density, Figs. 6c-d) reveal that the southern half of the transect (St. 91-98) was much more uniform vertically, and St. 96 and 97 were characterized by a fully overturned water column (Fig. 3b). This half of the section had more open water leads (89-92% ice concentration) and much weaker stratification (Fig. 6b), indicative of enhanced convection beneath the less concentrated sea ice.

Nutrient concentrations were high on the central shelf (9-14 µmol NO_3^- L^{-1}) and decreased to >0.4 µmol NO_3^- L^{-1} as bottom depth increased to ~200 m on the slope (Fig. 6e), due to both the difference in water mass properties and biological uptake. A modest under-ice phytoplankton bloom (~1 µg Chl *a* L^{-1}) extended ~80 km beneath the fully consolidated sea ice (St. 83-89) along this transect in waters with shallow MLDs relative to Z_{cr}. The diatom community within the bloom (St. 83 and 85) was dominated by water column phytoplankton (72 ± 8.9%) rather than ice-derived algae (28 ± 8.9%). Waters with more leads contained lower biomass (~0.3 µg Chl *a* L^{-1}) and had deeper MLDs relative to the shallower Z_{cr} (Fig. 6f). Oxygen (Fig. 6g) was highest (104%) in deeper waters on the slope, near saturation (96-103%) in the bloom, and undersaturated at the remaining stations. Fv:Fm (Fig. 6h) was highest (~0.5) in bloom waters and lowest (~0.3) at St. 96 and St. 97 where the water column was fully overturned. As with the Hanna Ridge section, these observations indicate that phytoplankton blooms occur under sea ice with snow where Z_{cr} exceeds the MLD.

3.4 Hydrographic and bio-physical relationships

3.4.1 Sea ice concentration, water column structure, nutrients, and phytoplankton

Across all 72 stations, lead fraction was negatively correlated with stratification index and ML slope and positively correlated with MLD and ML NO_3^- (Table 1) and water column (WC) NO_3^- (R=0.28; p<0.05). Thus, waters beneath sea ice with leads were less stratified with deeper and more homogeneous mixed layers containing more nutrients, indicative of mixing to the bottom. Similarly, stratification index was positively correlated with ML slope (Table 1) and inversely correlated with ML NO_3^- (Table 1) and WC NO_3^- concentrations (R=-0.52; p<0.01). The mean stratification index at stations with few to no leads (≥98% ice concentration; n=24) was >3-fold greater (p<0.01) than at stations with relatively more leads (84-98% ice concentration; n=48), with means of 0.71 ± 0.85 kg m^{-3} and 0.22 ± 0.16 kg m^{-3}, respectively. Similarly, mean ML slope was >4-fold greater (p<0.001) beneath ice with few to no leads. Thresholds of 100% or ≥95% to categorize stations with few to no leads yielded similar patterns. These results are consistent with convective overturning via brine rejection when leads open in the ice and begin to freeze.

Correlations between ML Chl *a*, lead fraction, and stratification index (Table 2) illustrate that phytoplankton biomass was higher in more stable waters with fewer leads. Biomass was not correlated with ML NO_3^- or with ML slope. Fv:Fm was positively correlated with stratification index (Table 2), demonstrating higher photosynthetic efficiencies in more stable waters. O_2 saturation was higher in more stratified waters with fewer leads (Table 2). Z_{cr} was positively correlated with stratification index and inversely correlated with MLD (Table 2). Consistent with observations, Z_{cr}:MLD was positively correlated with Fv:Fm (0.53; p<0.01; N=38) and O_2 saturation (R=0.42; p<0.01; N=72), but not correlated with lead fraction, stratification index, or ML NO_3^-. Chl *a* was used to calculate Z_{cr}, so its correlation with Z_{cr}:MLD was omitted.

3.4.2 Under-ice phytoplankton response to environmental conditions

To assess how under-ice phytoplankton are influenced by complex interactions between physical and biogeochemical properties, we constructed a multiple linear regression model

(Table 3), using log-transformed ML Chl *a* as the biological response variable. Lead fraction, stratification index, MLD, and ML NO_3^- were assigned as environmental predictors. The model was statistically significant ($R^2 = 0.31$; $p<0.001$), illustrating that these predictor variables explained 31% of the variance in ML Chl *a* across the 72 stations. The most important factor controlling phytoplankton biomass was MLD, which contributed 39.0% of the explained variance. Stratification index and lead fraction were next in importance, contributing 27.7% and 27.2% of the explained variance, respectively, although lead fraction was significant only at the 90% significance level. The least important factor was ML NO_3^-, which was available at all stations and contributed 6.1% of the explained variance. ML slope was not correlated with phytoplankton biomass and was removed from the multiple linear regression model.

3.5 Theoretical model of irradiance, primary production, and critical depth in sea ice with leads

Consistent with the SUBICE field observations demonstrating the presence of modest under-ice phytoplankton blooms beneath fully consolidated sea ice with snow, our theoretical model demonstrates that light availability is sufficient for under-ice blooms to develop from pre-bloom concentrations even beneath 100% ice cover. Modeled surface light beneath 100% ice cover with snow ranged over the daily cycle from 4 to 60 µEin m^{-2} s^{-1}, corresponding to ~3% transmission. These values compare well with radiometer measurements of bottom ice irradiance during SUBICE [*Selz et al.*, 2017]. For example, bottom ice irradiance at solar noon was ~40 µEin m^2 s^{-1} beneath 1.41 m thick ice with 0.08 m snow depth and ~100 µEin m^2 s^{-1} beneath 0.98 m thick ice with 0.06 m snow depth. We note that snow depth greatly affects light transmission. Simulated light transmission through bare ice is much higher (~13%; up to ~260 µEin m^{-2} s^{-1}), consistent with field measurements from ICESCAPE (12.7 – 17.5%; *Arrigo et al.* [2014]) and in the Canadian Arctic (5-16%; *Ehn et al.* [2011]). Conversely, with our maximum observed snow cover (0.15 m), simulated light is reduced to ~10 µEin m^{-2} s^{-1} due to strong attenuation by snow, consistent with *Perovich et al.* [1998]. The modeled surface light in leads of open water ranged from 40 to ~1900 µEin m^{-2} s^{-1} over the daily cycle.

Beneath 100% ice cover with snow, GPP exceeded community respiration in the upper 4 m of the water column, yielding a Z_{cr} of 6.6 m (Fig. 7a). Thus, there is enough light in surface waters beneath fully consolidated sea ice with moderate to low snow cover for a bloom to begin in the absence of active mixing deeper than Z_{cr}. However, if the water column is actively mixed beyond Z_{cr}, community respiration would exceed GPP in the upper ML and prevent bloom development. Additionally, increased snow cover (or older, thicker sea ice) would prevent bloom development through shoaling of Z_{cr} due to the attenuation of sunlight, while reduced snow cover (or very thin ice) would deepen Z_{cr}, making the water column more favorable for blooms.

As the presence of leads increases, irradiance in the water column also increases, resulting in greater estimates of GPP relative to respiration and deeper Z_{cr}. At ice concentrations of 96, 92, and 83%, Z_{cr} was 10 m, 14 m (Fig. 7b), and 23 m (Fig. 7c), respectively. As ice concentration varied from 100% (no leads) to 0% (completely ice-free waters), Z_{cr} increased from several meters to 150 m (Fig. 7d). The ice concentration at which Z_{cr} exceeded the mean bottom depth (50 m) for waters on the shallow Chukchi shelf was 67%. Thus, at greater ice concentrations, complete overturning of the water column results in vertical mixing deeper than Z_{cr}, preventing under-ice bloom development. These findings are consistent with our field results, illustrating that phytoplankton can bloom in the absence of mixing even at very high ice concentration with snow, while convective mixing in leads can prevent bloom development.

4 Discussion

4.1 Modest under-ice blooms even beneath fully consolidated sea ice

A particularly noteworthy outcome of the SUBICE expedition is the finding of modest phytoplankton blooms (~1-3 μg Chl *a* L^{-1}) beneath 100% sea ice with snow. These surprising field observations were supported by our theoretical model calculations, which demonstrate that first-year sea ice transmits sufficient light for phytoplankton blooms to develop near the surface of a stable water column, even with low-to-moderate snow cover. Although only ~30% of the study region was characterized by sea ice with no or few leads during SUBICE, observations from these locations indicate that blooms can begin beneath snow-covered first-year ice prior to melt pond formation. Bloom development beneath snow-covered sea ice requires a lack of active mixing within the upper ML, consistent with our observations of a stable water column at ~100% ice cover. If the water column is actively mixed via convection or another process, a bloom cannot develop from pre-bloom concentrations. However, as phytoplankton biomass increases, primary production and z_{cr} also increase, such that once an under-ice bloom begins in surface waters, bloom development can continue even with increased mixing.

Conversely, reduced light from thicker sea ice or more snow would result in a shallower $Z_{cr,}$ limiting bloom development. While enhanced stratification at the shelfbreak front may have contributed to bloom development in the Central Shelf transect, waters were relatively weakly stratified across the Chukchi shelf. We find no evidence that the water column stability supporting under-ice phytoplankton growth in shelf waters was determined by enhanced stratification due to solar heating, snow melt, or large-scale horizontal advection. Rather, the water column is likely more stable due to a lack of vertical mixing beneath the sea ice which leads to restratification via small scale processes such as horizontal mixing.

It is important to consider the contribution of sea ice algae sloughing off the bottom of the ice into the water column, thereby elevating the biomass beneath snow-covered sea ice. In our field observations, the available community composition data revealed that the under-ice bloom diatom communities were composed primarily of water column phytoplankton rather than sea ice-derived algal diatoms. We can estimate the potential contribution of biomass derived from sea ice algae to the water column assuming the rapid release of a 0.02 m^{-1} layer of sea ice algae with 1,000 µg Chl a L^{-1} (the maximum biomass sampled during SUBICE). For a 26 m MLD (the mean for the under-ice bloom at Hanna Ridge St. 37-39; Fig. 4), the maximum contribution to the upper ML would be 0.77 µg Chl a L^{-1}. This non-bloom concentration is lower than our observations (1-3 µg Chl a L^{-1}). Finally, high Fv:Fm in under-ice bloom waters indicates healthy phytoplankton rather than sloughed ice algae. The potential seeding of under-ice blooms by ice algae is further discussed by *Selz et al.* [2017].

Considering that melt ponds typically form only a few weeks before sea ice retreat [*Palmer et al.,* 2014], our findings suggest that the duration of under-ice phytoplankton blooms may be longer than previously realized. As we observed, light transmission through snow-covered sea ice may play an important role in increasing background phytoplankton concentrations, possibly contributing to the development of highly productive under-ice blooms several weeks later. Although field data were not obtained prior to melt pond formation at the site of the massive under-ice phytoplankton bloom observed during ICESCAPE [*Arrigo et al.,* 2012], the presence of a modest under-ice bloom beneath snow-covered ice would facilitate rapid subsequent accumulation of biomass once melt ponds form. Thus, the extraordinarily high depth-integrated biomass and nutrient depletion observed beneath ponded sea ice during ICESCAPE [*Arrigo et al.,* 2014] could have evolved from a more modest bloom prior to pond formation.

4.2 The role of leads for phytoplankton bloom development

This study addresses whether leads of open water play a similar role to melt ponds in transmitting sunlight for phytoplankton blooms in ice-covered waters. Our theoretical model results indicate that, even at very high ice concentration, leads substantially increase light penetration to the upper water column, implying that they should play an important role in facilitating the development of under-ice blooms. This concept is supported by a small number of previous observations of enhanced phytoplankton biomass beneath sea ice with leads [*English*, 1961; *Bursa*, 1963; *Gosselin et al.*, 1997; *Assmy et al.*, 2017]. However, to our surprise, we observed lower phytoplankton biomass beneath sea ice with leads than beneath ice with few to no leads, despite consistently high nutrient availability across the Chukchi shelf.

Although seemingly counterintuitive, this finding is consistent with our hydrographic observations, which revealed greater water column stability beneath fully consolidated sea ice than beneath sea ice with leads. By way of explanation, *Pacini et al.* [submitted] argued that refreezing of surface waters in leads drives convective overturning, as evidenced by short overturn times and a completely mixed water column at some of the SUBICE stations on the shelf. Leveraging their hydrographic analysis, we attribute our biological observations of relatively low phytoplankton biomass beneath leads to reduced stratification due to convective mixing in refreezing leads. Mixing to deeper depths reduces the mean light dose that phytoplankton receive in the upper mixed layer, resulting in a net decrease in Z_{cr} despite increased light transmission through leads. As in *Sverdrup* [1953], vertical mixing prevents blooms where MLD > Z_{cr}, consistent with the notion that the shutdown of turbulent convection triggers the onset of spring blooms at lower latitudes [e.g. *Taylor and Ferrari*, 2011]. These results demonstrate the pivotal role of springtime convective mixing in controlling phytoplankton bloom dynamics in the sea ice zone, complementing previous studies on the importance of convection for nutrients and hydrography during the initial freeze-up in autumn and in leads and polynyas during winter [*Smith and Morison*, 1993; *Weingartner et al.*, 1998; *Woodgate et al.*, 2005a; *Pickart et al.*, 2016].

On the other hand, as demonstrated by our theoretical model calculations, leads also act as ‘windows’ of light to the ice-covered water column and are therefore potentially important sites for enhanced primary production. We suggest the critical factor is the air-sea buoyancy forcing. In warmer atmospheric conditions when the surface water is not refreezing – either later in the season or in a warmer year – we expect that leads of open water play a similar role to melt ponds in increasing light transmission and supporting blooms in the sea ice zone. Additionally, once leads fully refreeze and convection ceases, light transmission through the relatively young and thin sea ice with reduced snow cover may also promote enhanced under-ice phytoplankton biomass, as observed by Assmy et al. [2017] in the Arctic Ocean north of Svalbard. Furthermore, at much greater lead concentrations, increased light transmission through open leads may support bloom formation despite convective mixing. Based on our theoretical model, for the shallow shelf waters (~50 m) of the Chukchi Sea, blooms may develop even during convective overturning due to increased light transmission at ice concentrations below 67%.

4.4 Implications for marine ecosystems in the changing Arctic Ocean

Sea ice conditions in the Arctic Ocean are being dramatically altered by climate change, with reductions in the thickness and age of sea ice accompanied by earlier ice retreat in recent decades (e.g. [*Kwok and Rothrock*, 2009; *Maslanik et al.*, 2011; *Stammerjohn et al.*, 2012]). The fate of polar marine ecosystems critically depends on the response of phytoplankton at the base of the food web to these abrupt changes in the physical environment. Recent field, satellite, and modeling work suggests that the timing of peak primary production in continental shelf regions of the Arctic Ocean may be shifting to earlier in the season due to earlier ice retreat [*Kahru et al.*, 2010] and the presence of under-ice phytoplankton blooms [*Arrigo et al.*, 2012; *Lowry et al.*, 2014; *Palmer et al.*, 2014; *Assmy et al.*, 2017]. Our observation of phytoplankton blooms in the sea ice zone in late spring provides more evidence for a potential shift in the timing of bloom development to earlier in the year, with critical yet poorly understood ecosystem implications.

Further, while the contribution of sea ice algae to under-ice primary production has been recognized for decades [*Horner and Schrader*, 1982; *Gosselin et al.*, 1997; *Gradinger*, 2009], the potential importance of water column phytoplankton beneath sea ice is only recently beginning to be understood. In most current estimates of net primary production in seasonally ice-covered regions (e.g. [*Pabi et al.*, 2008; *Arrigo et al.*, 2011; *Bélanger et al.*, 2013]), phytoplankton primary production beneath the ice is assumed to be negligible due to light limitation. The unexpectedly high accumulation of phytoplankton biomass beneath first-year sea ice in 2011 demonstrated the role of melt ponds in illuminating the water column for phytoplankton growth

[*Frey et al.*, 2011; *Arrigo et al.*, 2012], motivating additional studies of light transmission and phytoplankton bloom development beneath melt ponded sea ice [*Palmer et al.*, 2014; *Zhang et al.*, 2015]. Our findings reinforce the importance of accounting for under-ice primary production, demonstrating that even snow-covered sea ice can support the early development of modest phytoplankton blooms prior to melt pond formation. The contribution of these modest blooms to the total productivity of the Arctic Ocean and their role in the food web is presently unknown.

Likewise, while the importance of leads in sea ice has been documented as habitat for upper trophic levels such as polar bears and ringed seals (e.g. [*Stirling*, 1997]), their significance for phytoplankton in the sea ice zone has to date not been well characterized. Our study revealed that, in the Chukchi Sea, although leads increase light transmission to the underlying water column and have the potential to support under-ice primary production, convective mixing in refreezing leads can prevent bloom development. The prevalence and distribution of leads and the associated air-sea fluxes will likely play an important and previously unrecognized role in controlling spring phytoplankton bloom development in the future. However, more work is needed to understand the complex biophysical processes in the sea ice zone, both in the Chukchi Sea and in other Arctic regions. In the Laptev Sea, for example, weak stratification due to tidal mixing was found to prevent under-ice phytoplankton bloom development in waters with sufficient nutrient availability [*Janout et al.*, 2017]. Thus, considering the region-specific dynamics of the Arctic Ocean, more observations are needed during all seasons and across all sectors to fully characterize the different factors influencing phytoplankton bloom dynamics. Similarly, to better understand the ecosystem response to continued changes in sea ice, hydrographic conditions, and primary production, there is a critical need for additional field and modeling studies of higher trophic levels and food web dynamics in Arctic marine ecosystems.

Acknowledgments

We would like to acknowledge the captain, crew, and science party of the USCGC *Healy* for their contributions during cruise HLY1401, and two reviewers for their suggestions that greatly improved the manuscript. Fieldwork and analysis for the SUBICE program was supported by the National Science Foundation (NSF) Grant No. PLR-1304563 to KRA. Funding for KEL was provided through the NSF Graduate Research Fellowship Program (Grant No. DGE-0645962) and the Stanford University Gerald J. Lieberman Fellowship. RSP, AP, and CN were supported by NSF Grant No. PLR-1303617. Data can be found on the SUBICE website: www.ocean.stanford.edu/subice.

References

Ardyna, M., M. Babin, M. Gosselin, E. Devred, L. Rainville, and J.-E. Tremblay (2014), Recent Arctic Ocean sea ice loss triggers novel fall phytoplankton blooms, *Geophys. Res. Lett.*, *41*(17), 6207–6212, doi:10.1002/2014GL061047.

Armstrong, F., C. R. Stearns, and J. Strickland (1967), The measurement of upwelling and subsequent biological process by means of the Technicon Autoanalyzer® and associated equipment, *Deep-Sea Res.*, *14*, 381–389, doi:10.1016/0011-7471(67)90082-4.

Arrigo, K. R. et al. (2014), Phytoplankton blooms beneath the sea ice in the Chukchi Sea, *Deep-Sea Res. II, 105*, 1–16, doi:10.1016/j.dsr2.2014.03.018.

Arrigo, K. R., and G. L. van Dijken (2015), Continued increases in Arctic Ocean primary production, *Prog. Oceanogr.*, *136*(C), 60–70, doi:10.1016/j.pocean.2015.05.002.

Arrigo, K. R., et al. (2012), Massive phytoplankton blooms under Arctic sea ice, *Science*, *336*, 1408–1408, doi:10.1126/science.1215065.

Arrigo, K. R., G. L. van Dijken, and S. Pabi (2008), Impact of a shrinking Arctic ice cover on marine primary production, *Geophys. Res. Lett.*, *35*(19), L19603, doi:10.1029/2008GL035028.

Arrigo, K. R., M. M. Mills, G. L. van Dijken, K. E. Lowry, R. S. Pickart, and R. Schlitzer (2017), Late Spring Nitrate Distributions Beneath the Ice-Covered Northeastern Chukchi Shelf, *Journal of Geophysical Research: Biogeosciences*, *95*(17), 18,163–9, doi:10.1002/2017JG003881.

Arrigo, K. R., M. M. Mills, L. R. Kropuenske, G. L. van Dijken, A.-C. C. Alderkamp, and D. H. Robinson (2010), Photophysiology in Two Major Southern Ocean Phytoplankton Taxa: Photosynthesis and Growth of Phaeocystis antarctica and Fragilariopsis cylindrus under Different Irradiance Levels, *Integrative and Comparative Biology*, *50*(6), 950–966, doi:10.1093/icb/icq021.

Arrigo, K. R., P. A. Matrai, and G. L. van Dijken (2011), Primary productivity in the Arctic Ocean: Impacts of complex optical properties and subsurface chlorophyll maxima on large-scale estimates, *J. Geophys. Res.*, *116*, C11022–C11022.

Assmy, P. et al. (2017), Leads in Arctic pack ice enable early phytoplankton blooms below snow-covered sea ice, *Sci. Rep.*, 1–9, doi:10.1038/srep40850.

Belsley, D. A., E. Kuh, and R. E. Welsch (1980), *Detecting and assessing collinearity*, Identifying Influential Data and Sources of Collinearity, John Wiley & Sons, Inc., Hoboken, NJ, USA.

Bélanger, S., M. Babin, and J. E. Tremblay (2013), Increasing cloudiness in Arctic damps the increase in phytoplankton primary production due to sea ice receding, *Biogeosciences*.

Brown, Z. W., K. Lowry, M. A. Palmer, and G. L. van Dijken (2015), Characterizing the subsurface chlorophyll a maximum in the Chukchi Sea and Canada Basin, *Deep-Sea Res. II*, *118*, 88–104.

Bursa, A. (1963), Phytoplankton in coastal waters of the Arctic Ocean at Point Barrow, Alaska, *Arctic*, doi:10.2307/40507208.

Cavalieri, D. J., C. L. Parkinson, P. Gloersen, and H. J. Zwally (1996), Sea Ice Concentrations from Nimbus-7 SMMR and DMSP SSM/I-SSMIS Passive Microwave Data, Version 1.1, *NASA National Snow and Ice Data Center Distributed Active Archive Center*, doi:http://dx.doi.org/10.5067/8GQ8LZQVL0VL. Date Accessed: 16 December 2015.

Codispoti, L. A., C. Flagg, V. Kelly, and J. H. Swift (2005), Hydrographic conditions during the 2002 SBI process experiments, *Deep-Sea Res. II*, *52*(24-26), 3199–3226.

Codispoti, L. A., C. N. Flagg, and J. H. Swift (2009), Hydrographic conditions during the 2004 SBI process experiments, *Deep-Sea Res. II*, *56*(17), 1144–1163.

Cooper, L. W., T. E. Whitledge, J. M. Grebmeier, and T. Weingartner (1997), The nutrient, salinity, and stable oxygen isotope composition of Bering and Chukchi Seas waters in and near the Bering Strait, *J. Geophys. Res.*, *102*(C6), 12563–12573.

Corlett, W. B., and R. S. Pickart (2017), The Chukchi slope current, *Prog. Oceanogr.*, *153*, 50–65, doi:10.1016/j.pocean.2017.04.005.

Cota, G. F., L. R. Pomeroy, W. G. Harrison, E. P. Jones, F. Peters, W. M. Sheldon, and T. R. Weingartner (1996), Nutrients, primary production and microbial heterotrophy in the southeastern Chukchi Sea: Arctic summer nutrient depletion and heterotrophy, *Mar. Ecol. Prog. Ser.*, *135*(1-3), 247–258.

Cottrell, M. T., R. R. Malmstrom, V. Hill, and A. E. Parker (2006), The metabolic balance between autotrophy and heterotrophy in the western Arctic Ocean, *Deep-Sea Res I*, *53*(11), 1831–1844, doi:10.1016/j.dsr.2006.08.010.

Cullen, J. J., and R. F. Davis (2003), The blank can make a big difference in oceanographic measurements, *Limnol. Oceanogr. Bull.*, *12*(29), 29–35.

Ehn, J. K., C. J. Mundy, D. G. Barber, H. Hop, A. Rossnagel, and J. Stewart (2011), Impact of horizontal spreading on light propagation in melt pond covered seasonal sea ice in the Canadian Arctic, *J. Geophys. Res.*, *116*(10), 2069–15, doi:10.1029/2010JC006908.

English, T. S. (1961), Some biological oceanographic observations in the central North Polar Sea drift station Alpha, 1957-1958,, *13*, 1–80, doi:10.1029/2001JC001057/full.

Fortier, M., L. Fortier, C. Michel, and L. Legendre (2002), Climatic and biological forcing of the vertical flux of biogenic particles under seasonal Arctic sea ice, *Mar. Ecol. Prog. Ser.*, *225*, 1–16, doi:10.3354/meps225001.

Frey, K. E., D. K. Perovich, and B. Light (2011), The spatial distribution of solar radiation under a melting Arctic sea ice cover, *Geophys. Res. Lett.*, *38*(22), L22501.

Fukuchi, M., K. Watanabe, A. Tanimura, T. Hoshiai, H. Sasaki, H. Satoh, and Y. Yamaguchi (1989), A phytoplankton bloom under sea ice recorded with a moored system in lagoon Saroma Ko, Hokkaido, Japan, *Proceedings of the NIPR Symposium on Polar Biology, 2,* 9–15.

Gong, D., and R. S. Pickart (2015), Summertime circulation in the eastern Chukchi Sea, *Deep-Sea Res. II*, *118*, 18–31, doi:10.1016/j.dsr2.2015.02.006.

Gong, D. and R. S. Pickart (2016), Early summer water mass transformation in the eastern Chukchi Sea. *Deep-Sea Research II*, *130*, 43-55, doi:10.1016/j.dsr2.2016.04.015.

Gosselin, M., M. Levasseur, P. A. Wheeler, R. A. Horner, and B. C. Booth (1997), New measurements of phytoplankton and ice algal production in the Arctic Ocean, *Deep-Sea Res. II*, *44*(8), 1623–1644.

Gradinger, R. (2009), Sea-ice algae: Major contributors to primary production and algal biomass in the Chukchi and Beaufort Seas during May/June 2002, *Deep-Sea Res. II*, *56*(17), 1201–1212.

Grebmeier, J. M. et al. (2015), Ecosystem characteristics and processes facilitating persistent macrobenthic biomass hotspots and associated benthivory in the Pacific Arctic, *Prog. Oceanogr.*, *136*(C), 92–114, doi:10.1016/j.pocean.2015.05.006.

Grömping, U. (2006), Relative importance for linear regression in R: the package relaimpo, *J. Stat. Softw.*, *17*(1).

Hameedi, M. J. (1978), Aspects of water column primary productivity in the Chukchi Sea during summer, *Mar. Biol.*, *48*(1), 37–46.

Hill, V., G. F. Cota, and D. Stockwell (2005), Spring and summer phytoplankton communities in the Chukchi and Eastern Beaufort Seas, *Deep-Sea Res. II*, *52*(24-26), 3369–3385, doi:10.1016/j.dsr2.2005.10.010.

Holm-Hansen, O., C. J. Lorenzen, R. W. Holmes, and J. D. H. Strickland (1965), Fluorometric determination of chlorophyll, *ICES Journal of Marine Science*, *30*(1), 3–15, doi:10.1093/icesjms/30.1.3.

Horner, R., and G. C. Schrader (1982), Relative contributions of ice algae, phytoplankton and benthic microalgae to primary production in nearshore regions of the Beaufort Sea, *Arctic*, *35*(4), 485–503.

Itoh, M. et al. (2015), Water properties, heat and volume fluxes of Pacific water in Barrow Canyon during summer 2010, *Deep-Sea Res I*, *102*(C), 43–54, doi:10.1016/j.dsr.2015.04.004.

Itoh, M., K. Shimada, T. Kamoshida, F. McLaughlin, E. Carmack, and S. Nishino (2012), Interannual variability of Pacific Winter Water inflow through Barrow Canyon from 2000 to 2006, *J Oceanogr*, *68*(4), 575–592.

Janout, M. A., J. Hölemann, A. M. Waite, T. Krumpen, W.-J. von Appen, and F. Martynov (2016), Sea-ice retreat controls timing of summer plankton blooms in the Eastern Arctic Ocean, *Geophys. Res. Lett.*, *43*(24), 12,493–12,501, doi:10.1002/2016GL071232.

Kahru, M., V. Brotas, M. Manzano-Sarabia, and B. G. Mitchell (2010), Are phytoplankton blooms occurring earlier in the Arctic? *Global Change Biology*, *17*(4), 1733–1739, doi:10.1111/j.1365-2486.2010.02312.x.

Kirk, J. T. O. (2010), *Light and Photosynthesis in Aquatic Ecosystems*, Cambridge University Press.

Kolber, Z. S., O. Prášil, and P. G. Falkowski (1998), Measurements of variable chlorophyll fluorescence using fast repetition rate techniques: defining methodology and experimental protocols, *Biochimica et Biophysica Acta (BBA) - Bioenergetics*, *1367*(1-3), 88–106, doi:10.1016/S0005-2728(98)00135-2.

Kwok, R., and D. A. Rothrock (2009), Decline in Arctic sea ice thickness from submarine and ICESat records: 1958–2008, *Geophys. Res. Lett.*, *36*(15), L15501.

Laney, S. R., and H. M. Sosik (2014), Phytoplankton assemblage structure in and around a massive under-ice bloom in the Chukchi Sea, *Deep-Sea Res. II*, *105*, 30–41, doi:10.1016/j.dsr2.2014.03.012.

Legendre, L., R. G. Ingram, and M. Poulin (2011), Physical Control of Phytoplankton Production under Sea Ice (Manitounuk Sound, Hudson Bay), *Canadian Journal of Fisheries and Aquatic Sciences*, doi:10.1139/f81-185.

Lewis, M. R., and J. C. Smith (1983), A small volume, short-incubation-time method for measurement of photosynthesis as a function of incident irradiance, *Mar. Ecol. Prog. Ser.*, *13*, 99–102.

Loeng, K. Brander, E. Carmack, S. Denisenko, K. Drinkwater, B. Hansen, K. Kovacs, P. Livingston, F. McLaughlin, and E. Sakshaug (2005), Marine Systems, in *Arctic Climate*

Impact Assessment, pp. 453–538, Cambridge University Press, Cambridge, UK.

Lowry, K. E., G. L. van Dijken, and K. R. Arrigo (2014), Evidence of under-ice phytoplankton blooms in the Chukchi Sea from 1998 to 2012, *Deep-Sea Res. II*, *105*, 105–117, doi:10.1016/j.dsr2.2014.03.013.

Lowry, K. E., R. S. Pickart, M. M. Mills, and Z. W. Brown (2015), The influence of winter water on phytoplankton blooms in the Chukchi Sea, *Deep-Sea Res. II*, *118*, 53–72, doi:10.1016/j.dsr2.2015.06.006.

Lowry, K. E. (2016), The influence of sea ice and hydrography on the timing, distribution, and intensity of phytoplankton blooms in the rapidly changing Chukchi Sea (Arctic Ocean), Ph.D. Thesis, p. 80-118, Stanford University, Stanford, CA, USA.

Martin, T., M. Steele, and J. Zhang (2014), Seasonality and long-term trend of Arctic Ocean surface stress in a model, *J. Geophys. Res.*, *119*(3), 1723–1738, doi:10.1002/2013JC009425.

Maslanik, J., J. Stroeve, C. Fowler, and W. Emery (2011), Distribution and trends in Arctic sea ice age through spring 2011, *Geophys. Res. Lett.*, *38*(13), L13502.

Mathis, J. T., R. S. Pickart, D. A. Hansell, D. Kadko, and N. R. Bates (2007), Eddy transport of organic carbon and nutrients from the Chukchi Shelf: Impact on the upper halocline of the western Arctic Ocean, *J. Geophys. Res.*, *112*(C5), 14485–14, doi:10.1029/2006JC003899.

Morel, A. (1988), Optical modeling of the upper ocean in relation to its biogenous matter content (Case I waters), J. Geophys. Res., 93(C9), 10749–10768.

Moran, S. B. et al. (2005), Seasonal changes in POC export flux in the Chukchi Sea and implications for water column-benthic coupling in Arctic shelves, *Deep-Sea Res. II*, *52*(24–26), 3427–3451.

Mundy, C. J. et al. (2009), Contribution of under-ice primary production to an ice-edge upwelling phytoplankton bloom in the Canadian Beaufort Sea, *Geophys. Res. Lett., 36*(17), doi:10.1029/2009GL038837.

Nguyen, D., R. Maranger, J.-E. Tremblay, and M. Gosselin (2012), Respiration and bacterial carbon dynamics in the Amundsen Gulf, western Canadian Arctic, *J. Geophys. Res.*, *117*(C9), C00G16, doi:10.1029/2011JC007343.

Pabi, S., G. L. van Dijken, and K. R. Arrigo (2008), Primary production in the Arctic Ocean, 1998–2006, *J. Geophys. Res.*, *113*(C8), doi:10.1029/2007JC004578.

Pacini, A., R. S. Pickart, G. W. K. Moore, C. Nobre, F. Bahr, K. Våge, and K. R. Arrigo (submitted), Characteristics and transformation of Pacific winter water on the Chukchi Sea shelf in late-spring. *Deep-Sea Res. II.*

Padman, L., and S. Erofeeva (2004), A barotropic inverse tidal model for the Arctic Ocean, *Geophys. Res. Lett.*, *31*(2), doi:10.1029/2003GL019003.

Palmer, M. A., B. T. Saenz, and K. R. Arrigo (2014), Impacts of sea ice retreat, thinning, and melt-pond proliferation on the summer phytoplankton bloom in the Chukchi Sea, Arctic Ocean, *Deep-Sea Res. II*, *105*, 85–104, doi:10.1016/j.dsr2.2014.03.016.

Palmer, M. A., G. L. van Dijken, B. G. Mitchell, B. J. Seegers, K. Lowry, M. M. Mills, and K. R. Arrigo (2013), Light and nutrient control of photosynthesis in natural phytoplankton populations from the Chukchi and Beaufort seas, Arctic Ocean, *Limnol. Oceangr.*, *58*(6), 2185–2205, doi:10.4319/lo.2013.58.6.2185.

Parkinson, C. L., and D. J. Cavalieri (2008), Arctic sea ice variability and trends, 1979–2006, *J. Geophys. Res.*, *113*(C7), C07003–28, doi:10.1029/2007JC004558.

Pegau, W. S., and C. A. Paulson (2001), The albedo of Arctic leads in summer, *Annals of Glaciology*, *33*(1), 221–224, doi:10.3189/172756401781818833.

Perrette, M., A. Yool, G. D. Quartly, and E. E. Popova (2011), Near-ubiquity of ice-edge blooms in the Arctic, *Biogeosciences*, *8*(2), 515–524, doi:10.5194/bg-8-515-2011.

Perovich, D. K. (1990), Theoretical estimates of light reflection and transmission by spatially complex and temporally varying sea ice covers, J. Geophys. Res., 95(C6), 9557–9567, doi:10.1029/JC095iC06p09557.

Perovich, D. K. (2002), Ultraviolet Radiation and the Optical Properties of Sea Ice and Snow, in *UV Radiation and Arctic Ecosystems*, vol. 153, pp. 73–89, Springer Berlin Heidelberg, Berlin, Heidelberg.

Perovich, D. K., C. S. Roesler, and W. S. Pegau (1998), Variability in Arctic sea ice optical properties, J. Geophys. Res., 103(C1), 1193–1208.

Pickart, R. S., and D. J. Torres (2002), Hydrography of the Labrador Sea during active convection, *J. Phys. Oceanogr*, *32*, 428–457, doi:10.1175/1520-0485(2002)032%3C0428:HOTLSD%3E2.0.CO;2.

Pickart, R. S., T. J. Weingartner, L. J. Pratt, S. Zimmermann, and D. J. Torres (2005), Flow of winter-transformed Pacific water into the Western Arctic, *Deep-Sea Res. II*, *52*(24-26), 3175–3198, doi:10.1016/j.dsr2.2005.10.009.

Pickart, R. S., L. J. Pratt, D. J. Torres, T. E. Whitledge, A. Y. Proshutinsky, K. Aagaard, T. A. Agnew, G. W. K. Moore, and H. J. Dail (2010), Evolution and dynamics of the flow through Herald Canyon in the western Chukchi Sea, *Deep-Sea Res. II*, *57*(1-2), 5–26, doi:10.1016/j.dsr2.2009.08.002.

Pickart, R. S., G. W. K. Moore, C. Mao, F. Bahr, C. Nobre, and T. J. Weingartner (2016), Circulation of winter water on the Chukchi shelf in early Summer, *Deep-Sea Res. II*, *130*(C), 56–75, doi:10.1016/j.dsr2.2016.05.001.

Pisareva, M. et al. (2015), The Relationship Between Patterns of Benthic Fauna and Zooplankton in the Chukchi Sea and Physical Forcing, *Oceanography*, *28*(3), 68–83, doi:10.5670/oceanog.2015.58.

Platt, T., C. L. Gallegos, and W. G. Harrison (1981), *Photoinhibition of photosynthesis in natural assemblages of marine phytoplankton*.

Schlitzer, R. (2014), Ocean Data View, *http://odv.awi.de*.

Selz, V., S. Laney, A. Arnsten, K. Lewis, K. E. Lowry, H. Joy-Warren, M. M. Mills, G. van Dijken, K. R. Arrigo (2017). Late spring and early summer ice algal community distributions and coupling with the phytoplankton across the Chukchi and adjacent Beaufort Sea. *Limnology and Oceanography*.

Sherr, B. F., and E. B. Sherr (2003), Community respiration/production and bacterial activity in the upper water column of the central Arctic Ocean, *Deep Sea Research Part I: Oceanographic Research Papers*, *50*(4), 529–542, doi:10.1016/S0967-0637(03)00030-X.

Smith, D. C., IV, and J. H. Morison (1993), A numerical study of haline convection beneath leads in sea ice, *J. Geophys. Res.*, *98*(C6), 1–15.

Spall, M. A., R. S. Pickart, P. S. Fratantoni, and A. J. Plueddemann (2008), Western Arctic Shelfbreak Eddies: Formation and Transport, *J. Phys. Oceanogr.*, *38*(8), 1644–1668, doi:10.1175/2007JPO3829.1.

Stammerjohn, S., R. Massom, D. Rind, and D. Martinson (2012), Regions of rapid sea ice change: An inter-hemispheric seasonal comparison, *Geophys. Res. Lett.*, *39*(6), L06501, doi:10.1029/2012GL050874.

Stirling, I. (1997), The importance of polynyas, ice edges, and leads to marine mammals and birds, *Journal of Marine Systems*, *10*(1-4), 9–21, doi:10.1016/S0924-7963(96)00054-1.

Strass, V. H., and E. M. Nöthig (1996), Seasonal shifts in ice edge phytoplankton blooms in the Barents Sea related to the water column stability, *Polar Biol.*, *16*(6), 409–422, doi:10.1007/BF02390423.

Sukhanova, I. N., M. V. Flint, L. A. Pautova, D. A. Stockwell, J. M. Grebmeier, and V. M. Sergeeva (2009), Phytoplankton of the western Arctic in the spring and summer of 2002: Structure and seasonal changes, *Deep-Sea Res. II*, *56*(17), 1223–1236, doi:10.1016/j.dsr2.2008.12.030.

Sverdrup, H. U. (1953), On conditions for the vernal blooming of phytoplankton, *Journal du Conseil International pour l'Exploration de la Mer*, (18), 287–295.

Taylor, J. R., and R. Ferrari (2011), Shutdown of turbulent convection as a new criterion for the onset of spring phytoplankton blooms, *Limnol. Oceangr.*, *56*(6), 2293–2307, doi:10.4319/lo.2011.56.6.2293.

Tremblay, J. E., and J. Gagnon (2009), The effects of irradiance and nutrient supply on the productivity of Arctic waters: a perspective on climate change, in *Influence of Climate Change on the Changing Arctic and Sub-Arctic Conditions*, edited by J. C. J. Nihoul and A. G. Kostianoy, pp. 73–93, Springer Science + Business Media B. V.

Våge, K., G. W. K. Moore, S. Jónsson, and H. Valdimarsson (2015), Water mass transformation in the Iceland Sea, *Deep-Sea Res I*, *101*(C), 98–109, doi:10.1016/j.dsr.2015.04.001.

Webb, W. L., M. Newton, and D. Starr (1974), Carbon dioxide exchange of Alnus rubra, *Oecologia*, *17*(4), 281–291, doi:10.1007/BF00345747.

Weingartner, T. J., D. J. Cavalieri, K. Aagaard, and Y. Sasaki (1998), Circulation, dense water formation, and outflow on the northeast Chukchi shelf, *J. Geophys. Res.*, *103*(C4), 7647–7661.

Willmes, S., and G. Heinemann (2016), Sea-Ice Wintertime Lead Frequencies and Regional Characteristics in the Arctic, 2003–2015, *Remote Sensing*, *8*(4), 1–15, doi:10.3390/rs8010004.

Woodgate, R. A., K. Aagaard, and T. J. Weingartner (2005a), A year in the physical oceanography of the Chukchi Sea: Moored measurements from autumn 1990–1991, *Deep-Sea Res. II*, *52*(24–26), 3116–3149.

Woodgate, R. A., K. Aagaard, J. H. Swift, K. K. Falkner, and W. M. J. Smethie (2005b), Pacific ventilation of the Arctic Ocean's lower halocline by upwelling and diapycnal mixing over the continental margin, *Geophys. Res. Lett.*, *32*(18), L18609, doi:10.1029/2005GL023999.

Yager, P. L., T. L. Connelly, B. Mortazavi, K. E. Wommack, N. Bano, J. E. Bauer, S. Opsahl, and J. T. Hollibaugh (2001), Dynamic bacterial and viral response to an algal bloom at subzero temperatures, *Limnol. Oceangr.*, 790–801.

Zhang, J., C. J. Ashjian, R. Campbell, and Y. H. Spitz (2015), The influence of sea ice and snow cover and nutrient availability on the formation of massive under-ice phytoplankton blooms in the Chukchi Sea, *Deep-Sea Res. II*, *118*, 122–135, doi:10.1016/j.dsr2.2015.02.008.

Table 1. Pearson's correlation matrix demonstrating relationships between physical and environmental properties, including Lead fraction (defined as the inverse of sea ice concentration), Stratification Index, Mixed Layer (ML) Slope, Mixed Layer Depth (MLD), and mean ML NO_3^-. Bold values indicate significance at $p<0.05$ (*) and $p<0.01$ (**) (N=72).

	Lead Frac. (%)	Strat. Index (kg m^{-3})	ML Slope (kg m^{-4})	MLD (m)	ML NO_3^- (μmol L^{-1})
Lead Frac. (%)	1.0	-	-	-	-
Strat. Index (kg m^{-3})	**-0.38*** **	1.0	-	-	-
ML Slope (kg m^{-4})	**-0.35*** **	**0.50*** **	1.0	-	-
MLD (m)	**0.24***	0.17	-0.12	1.0	-
ML NO_3^- (μmol L^{-1})	**0.33***	**-0.76*** **	**-0.49*** **	-0.14	1.0

Table 2. Pearson's correlation matrix demonstrating relationships between physical and environmental properties and mean biological properties in the upper mixed layer (ML), including phytoplankton biomass (Chl *a*) (N=72), physiology (Fv:Fm) (N=38), and oxygen saturation (O_2 Sat.) (N=72), as well as critical depth (Z_{cr}) (N=72). Bold values indicate significance at p<0.05 (*) and p<0.01 (**).

	Lead Frac. (%)	Strat. Index (kg m^{-3})	ML Slope (kg m^{-4})	MLD (m)	ML NO_3^- (µmol L^{-1})
ML Chl *a* (µg L^{-1})	**-0.36****	**0.30***	0.21	**-0.28***	-0.13
ML Fv:Fm	-0.10	**0.38****	0.14	-0.23	-0.28
ML O2 Sat. (%)	**-0.29***	**0.78****	**0.50****	-0.08	**-0.72****
Z_{cr} (m)	0.03	**0.33****	0.17	**-0.24***	-0.18

Table 3. Multiple linear regression parameter estimates (± standard error) and relative importance of environmental predictors in explaining the variance in log-transformed mean Chl *a* in the upper mixed layer (N=72 stations). Bold values indicate significance ($p<0.05$). Although the intercept was only significant at the 91% confidence interval, the model was significant at $p<0.001$ ($R^2=0.31$).

Parameter	Estimate β	p-value	Relative Importance (%)
Intercept	-0.70 ± 0.41	0.09	
Lead Fraction (%)	-0.04 ± 0.02	0.10	27.2%
Stratification Index (kg m^{-3})	**0.53 ± 0.19**	**<0.01**	**27.7%**
Mixed Layer Depth (m)	**-0.02 ± 0.01**	**<0.01**	**39.0%**
Mixed Layer NO_3^- (μmol L^{-1})	0.04 ± 0.03	0.17	6.1%

Figure 1. Photographs of (**a**) melt-ponded sea ice, (**b**) waters characterized by a massive under-ice phytoplankton bloom, (**c**) sea ice with leads, and (**d**) waters characterized by low phytoplankton biomass beneath sea ice. Image credits: (**a**, **b**, and **d**) NASA ICESCAPE Team and (**c**) NASA ARISE Mission (https://earthobservatory.nasa.gov/blogs/fromthefield/2014/09/24/picturing-sea-ice-with-arises-digital-camera-instrument/).

Figure 2. Bathymetric map of the Chukchi Sea, including schematic flow paths of Pacific-origin water (after Corlett and Pickart [2017]). The locations of the 72 stations considered in the study are indicated by large circles, with colored stations illustrating the three transects presented in detail in Figs. 4-6: Hanna Ridge (HR; red), Chukchi Northwest (CNW; orange), and Central Shelf (CEN; yellow). The remaining SUBICE stations (black circles) were excluded due to possible influence by the northward advection of an open water bloom.

Figure 3. Maps of physical properties at each station in the Chukchi Sea during the SUBICE cruise. (**a**) Sea Ice Concentration (%), (**b**) Stratification Index (kg m^{-3}), (**c**) Mixed Layer Depth (MLD) (m), and (**d**) Critical Depth (Z_{cr}) (m). Bathymetric contours are labeled for 40, 50, 100, and 500 m. Fully overturned stations (stratification index ≤ 0.01 kg m^{-3}) are marked with asterisks on (**b**).

Figure 4. Hydrographic sections for the Hanna Ridge transect, sampled 22-23 May 2014. (**a**) Map illustrating the transect location, with labels for the first and last stations of the section. (**b**) Sea ice concentration (%) and stratification index (kg m^{-3}) at each station along the section. (**c**) θ (°C) with station labels. (**d**) Salinity with labeled potential density contours (kg m^{-3}) and station labels. (**e**) NO_3^- concentration (μmol L^{-1}). (**f**) Chl *a* concentration (mg L^{-1}) overlain with MLD (magenta dotted line) and Zcr (grey dotted line). (g) O2 saturation (%). (h) Fv:Fm.

Figure 5. The Chukchi Northwest transect, sampled 24-25 May 2014. See description of Fig. 4 above.

Figure 6. The Central Shelf transect, sampled 30 May - 2 June 2014. See description of Fig. 4 above.

Figure 7. Theoretical model of under-ice irradiance, gross primary production, and critical depth (Zcr) at varied lead fraction. (a, b, c) Theoretical profiles of production (solid green line with shading for mean ± standard deviation of 50,000 model simulations), respiration (solid red line), and Zcr (dotted blue line) at (a) 100% ice concentration, (b) 92% ice concentration, and (c) 83% ice concentration. (d) Theoretical Zcr (solid blue line with shading for mean ± standard deviation) at varied ice concentration (0-100%).

Figure 1.

(a) Melt-ponded sea ice

(b) Under-ice phytoplankton bloom

(c) Sea ice with leads

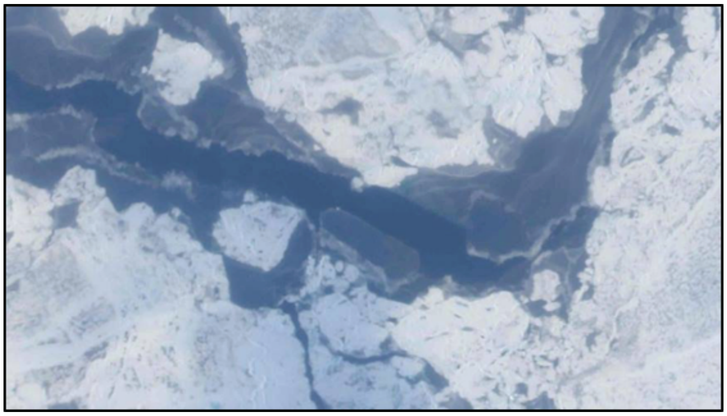

(d) Low phytoplankton biomass beneath sea ice

Figure 2.

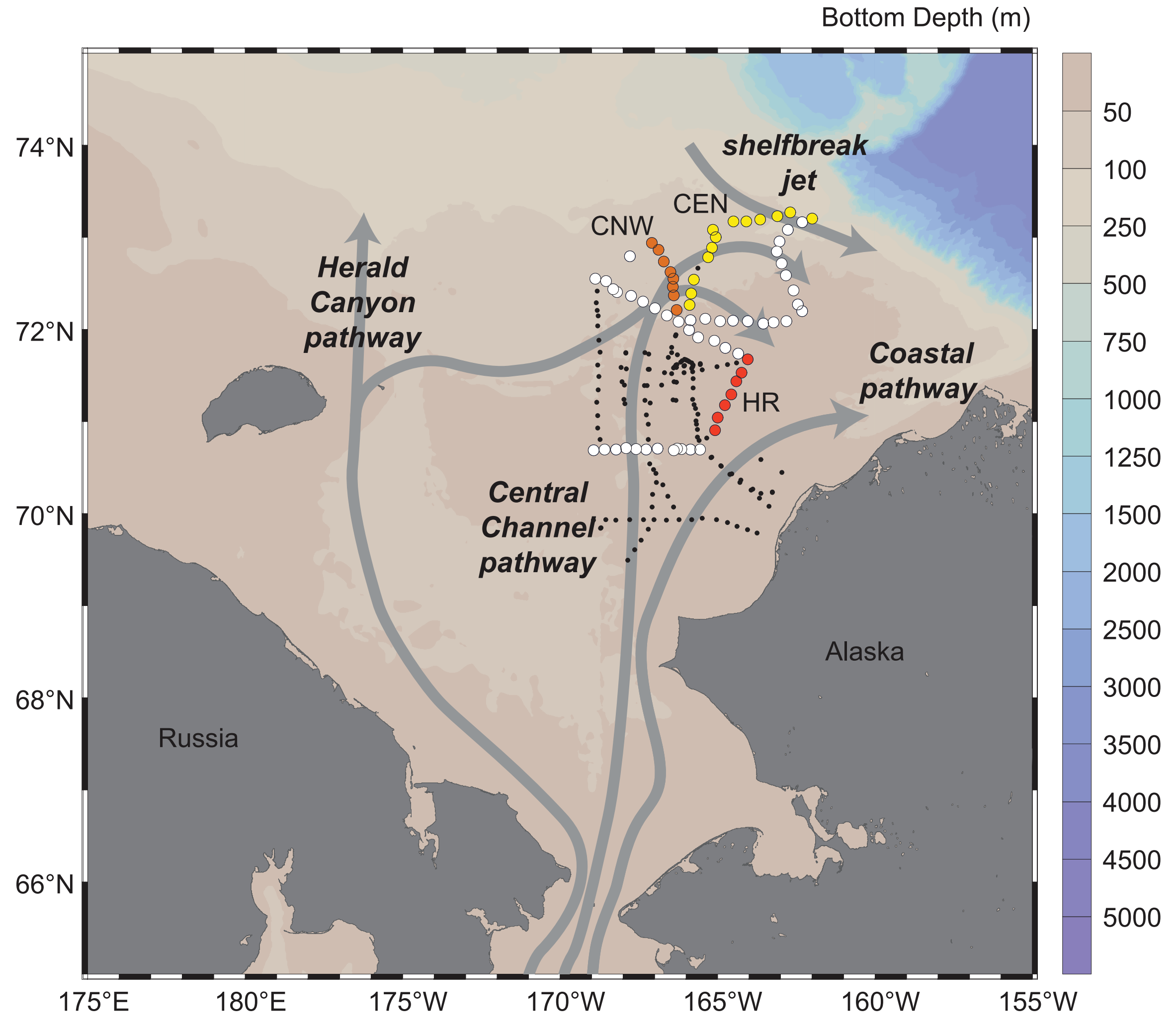
Bottom Depth (m)
50
100
250
500
750
1000
1250
1500
2000
2500
3000
3500
4000
4500
5000
74°N
72°N
70°N
68°N
66°N
175°E
180°E
175°W
170°W
165°W
160°W
155°W
shelfbreak jet
CEN
CNW
Herald Canyon pathway
Coastal pathway
HR
Central Channel pathway
Alaska
Russia

Figure 3.

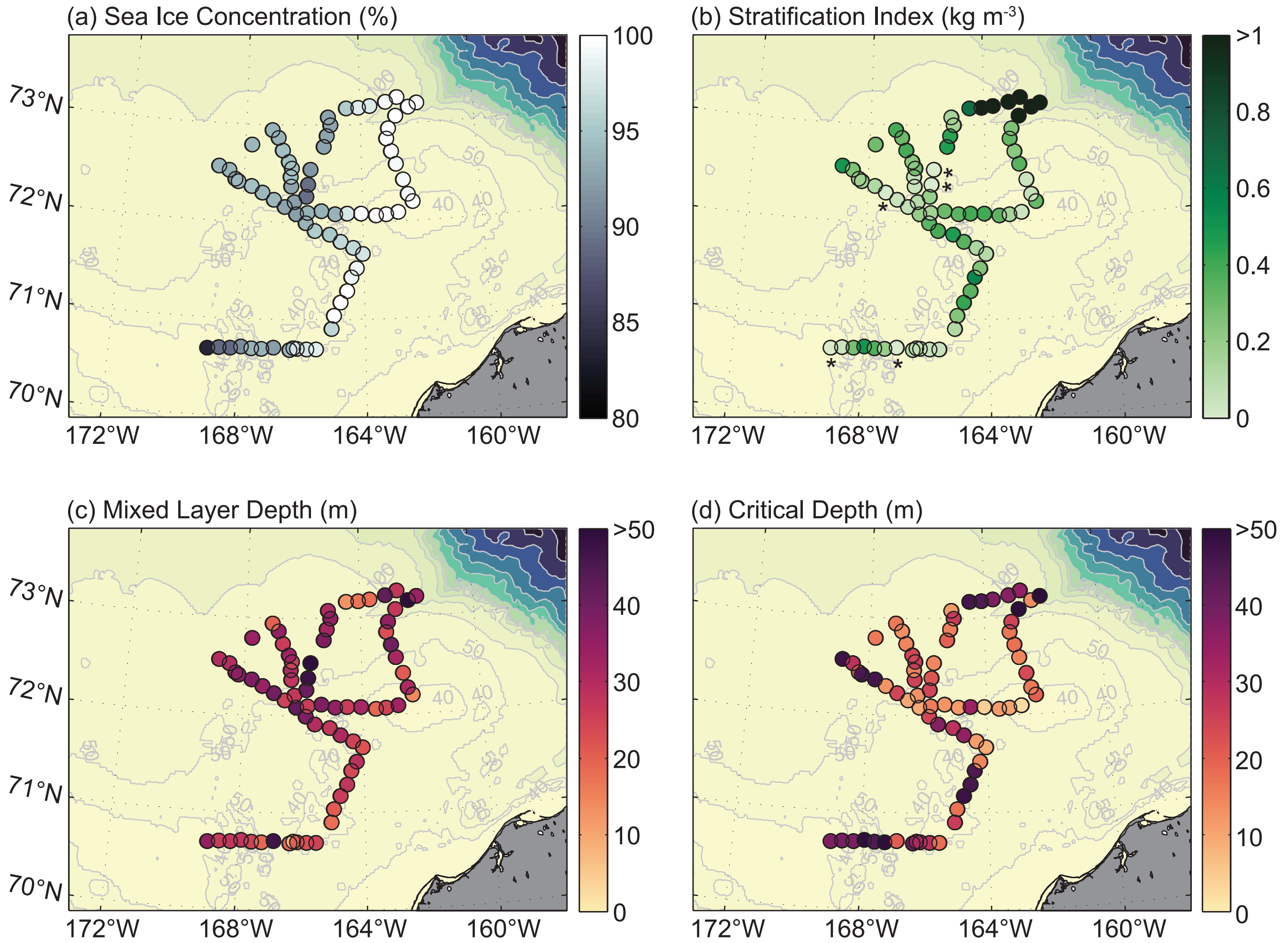
(a) Sea Ice Concentration (%)
(b) Stratification Index (kg m^{-3})
(c) Mixed Layer Depth (m)
(d) Critical Depth (m)
73°N
72°N
71°N
70°N
172°W
168°W
164°W
160°W
100
95
90
85
80
>1
0.8
0.6
0.4
0.2
0
>50
40
30
20
10
0
100
50
40
*

Figure 4.

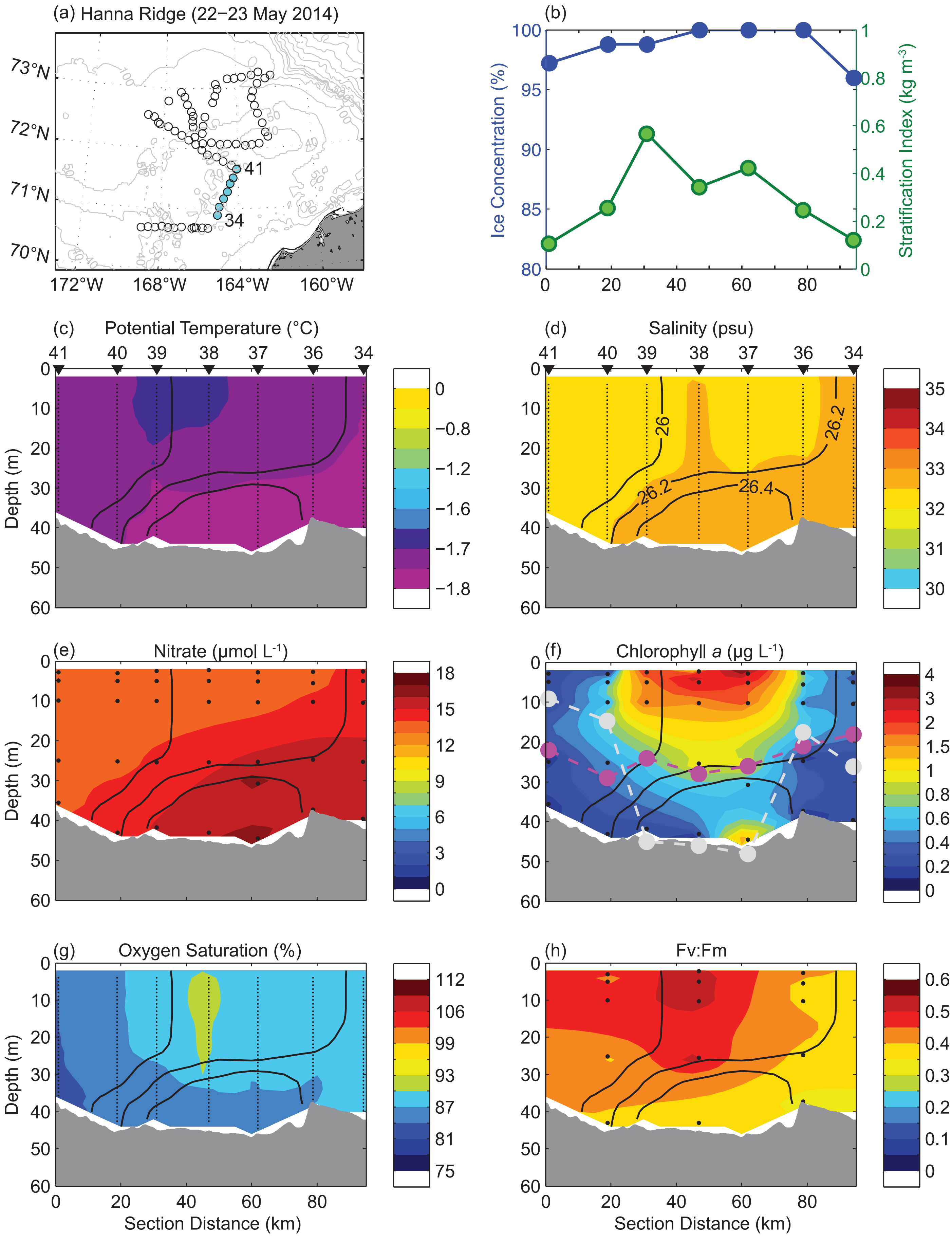
(a) Hanna Ridge (22–23 May 2014)
73°N
72°N
71°N
70°N
172°W
168°W
164°W
160°W
41
34
(b)
Ice Concentration (%)
Stratification Index (kg m⁻³)
100
95
90
85
80
1
0.8
0.6
0.4
0.2
0
0
20
40
60
80
(c) Potential Temperature (°C)
41
40
39
38
37
36
34
Depth (m)
0
−0.8
−1.2
−1.6
−1.7
−1.8
(d) Salinity (psu)
26
26.2
26.4
35
34
33
32
31
30
(e) Nitrate (μmol L⁻¹)
18
15
12
9
6
3
0
(f) Chlorophyll a (μg L⁻¹)
4
3
2
1.5
1
0.8
0.6
0.4
0.2
0
(g) Oxygen Saturation (%)
112
106
99
93
87
81
75
(h) Fv:Fm
0.6
0.5
0.4
0.3
0.2
0.1
0
0
10
20
30
40
50
60
Section Distance (km)

Figure 5.

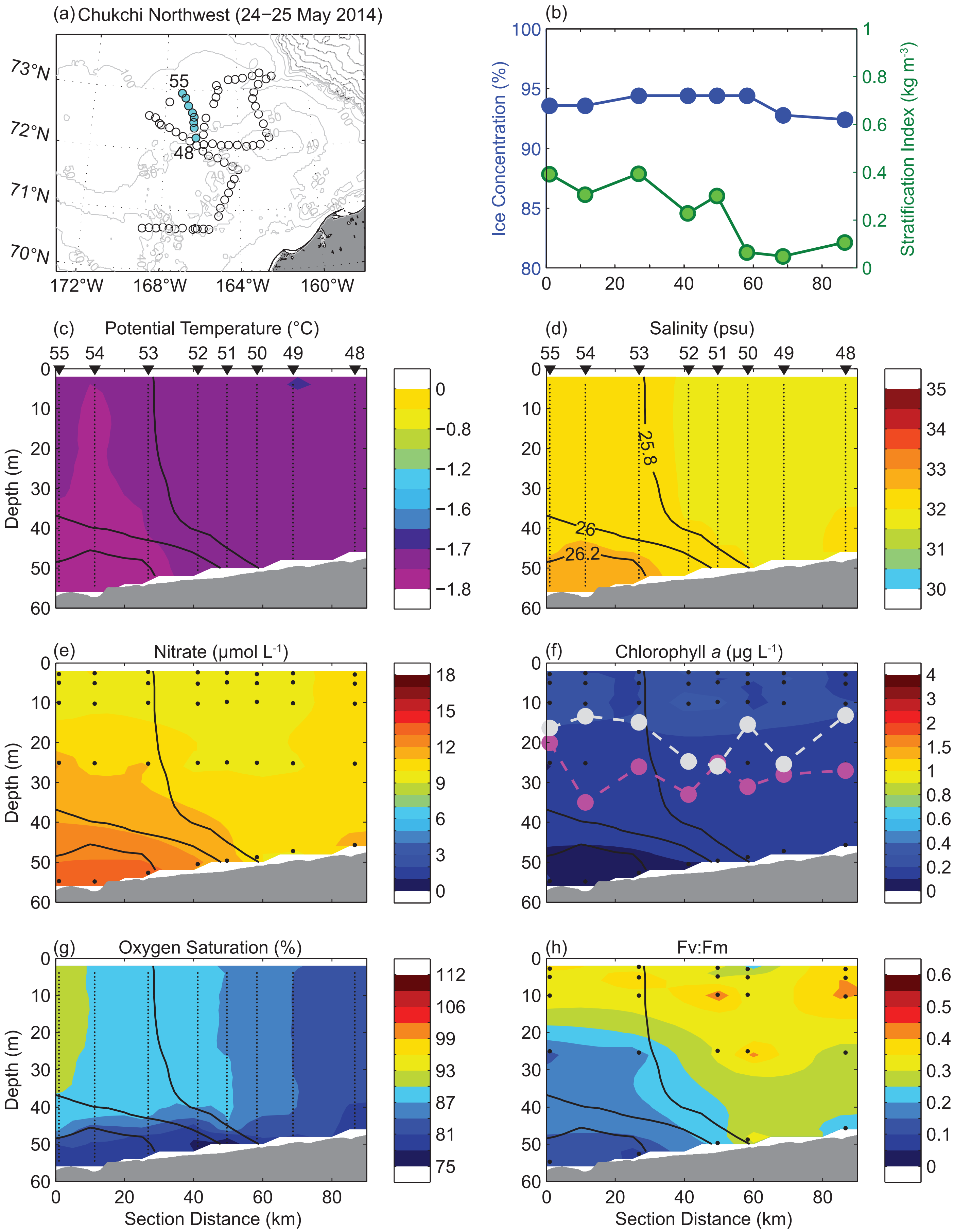
(a) Chukchi Northwest (24−25 May 2014)
73°N
72°N
71°N
70°N
172°W
168°W
164°W
160°W
55
48
(b)
Ice Concentration (%)
Stratification Index (kg m^{-3})
100
95
90
85
80
1
0.8
0.6
0.4
0.2
0
0
20
40
60
80
(c) Potential Temperature (°C)
55 54 53 52 51 50 49 48
Depth (m)
0
−0.8
−1.2
−1.6
−1.7
−1.8
(d) Salinity (psu)
55 54 53 52 51 50 49 48
25.8
26
26.2
35
34
33
32
31
30
(e) Nitrate (μmol L^{-1})
18
15
12
9
6
3
0
(f) Chlorophyll a (μg L^{-1})
4
3
2
1.5
1
0.8
0.6
0.4
0.2
0
(g) Oxygen Saturation (%)
112
106
99
93
87
81
75
(h) Fv:Fm
0.6
0.5
0.4
0.3
0.2
0.1
0
Depth (m)
0
10
20
30
40
50
60
Section Distance (km)
0
20
40
60
80

Figure 6.

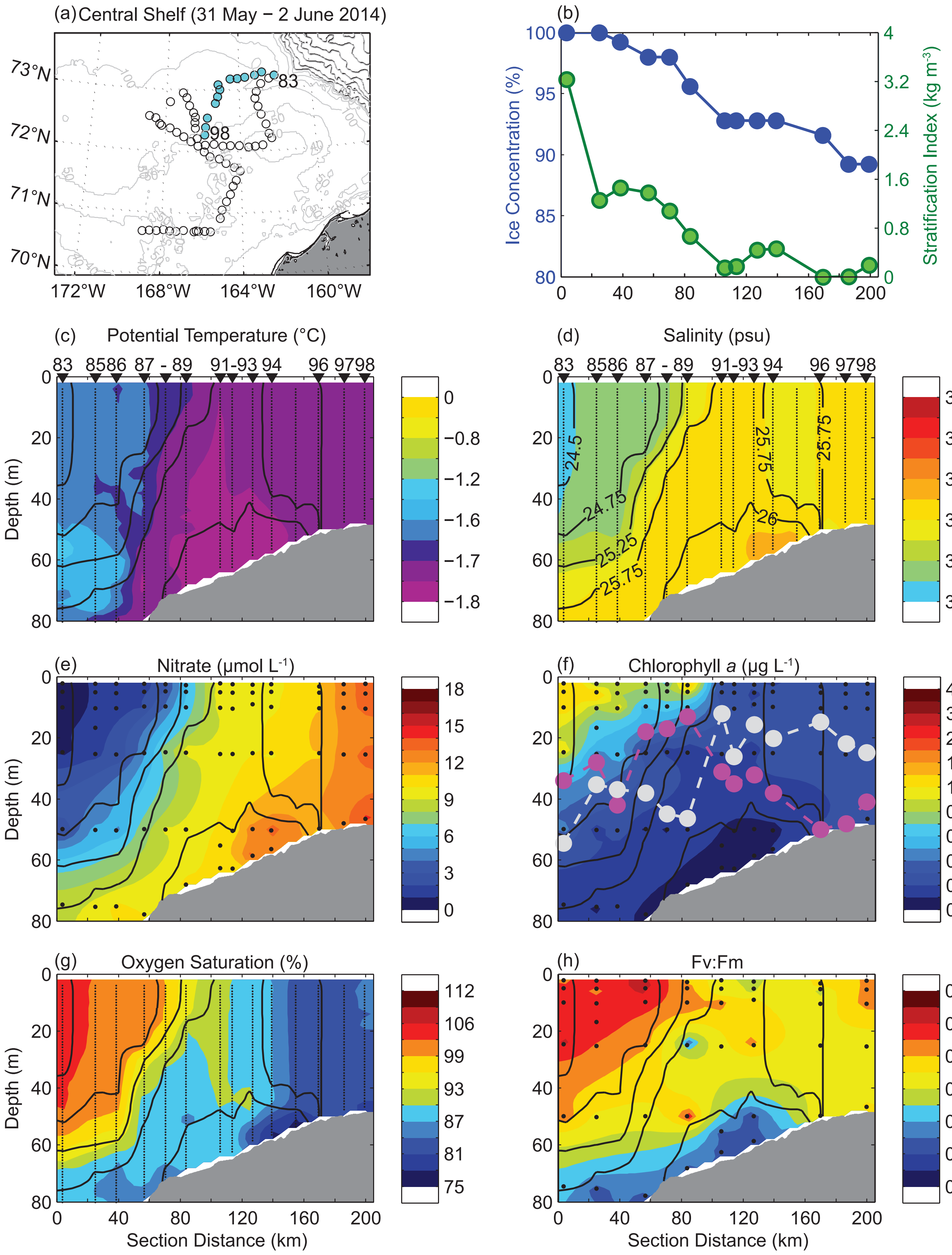
(a) Central Shelf (31 May − 2 June 2014)
73°N
72°N
71°N
70°N
172°W
168°W
164°W
160°W
83
98
(b)
Ice Concentration (%)
Stratification Index (kg m^{-3})
100
95
90
85
80
4
3.2
2.4
1.6
0.8
0
0
40
80
120
160
200
(c) Potential Temperature (°C)
83 8586 87 - 89 91-93 94 96 9798
Depth (m)
0
20
40
60
80
0
−0.8
−1.2
−1.6
−1.7
−1.8
(d) Salinity (psu)
83 8586 87 - 89 91-93 94 96 9798
24.5
24.75
25.25
25.75
26
35
34
33
32
31
30
(e) Nitrate (µmol L^{-1})
18
15
12
9
6
3
0
(f) Chlorophyll *a* (µg L^{-1})
4
3
2
1.5
1
0.8
0.6
0.4
0.2
0
(g) Oxygen Saturation (%)
112
106
99
93
87
81
75
(h) Fv:Fm
0.6
0.5
0.4
0.3
0.2
0.1
0
Section Distance (km)
0
40
80
120
160
200

Figure 7.

(a) Ice Concentration: 100%

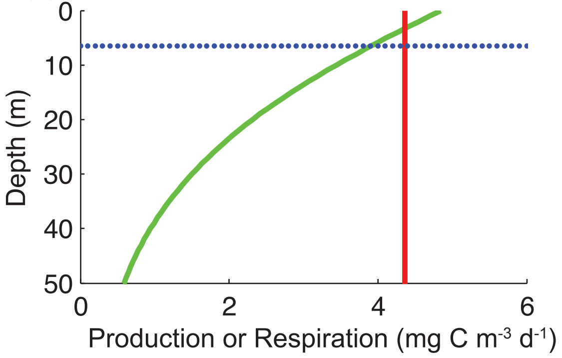

(b) Ice Concentration: 92%

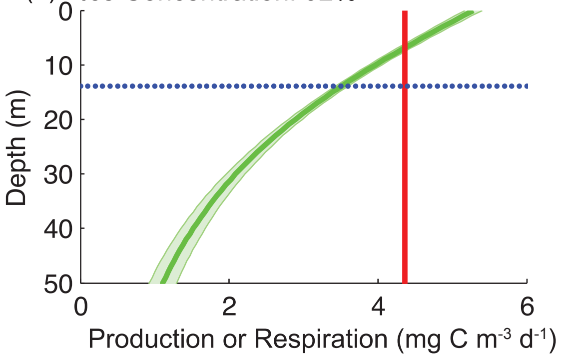

(c) Ice Concentration: 83%

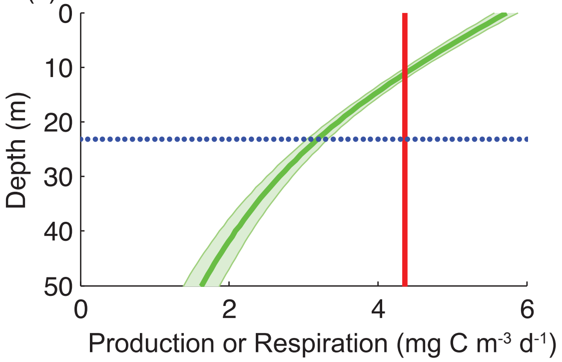

(d) Theoretical Critical Depth (m)